Research Paper

# The tobacco phosphatidylethanolamine-binding protein NtFT4 increases the lifespan of *Drosophila melanogaster* by interacting with the proteostasis network

**Philip Känel[1], Gundula A. Noll[2], Katrin Schroedter[1], Elke Naffin[3], Julia Kronenberg[1], Franziska Busswinkel[1], Richard M. Twyman[4], Christian Klämbt[3], Dirk Prüfer[1,2]**

[1]Fraunhofer Institute for Molecular Biology and Applied Ecology IME, Münster, Germany
[2]Institute of Plant Biology and Biotechnology, University of Münster, Münster, Germany
[3]Institute of Neuro- and Behavioral Biology, University of Münster, Münster, Germany
[4]TRM Ltd, Scarborough, United Kingdom

**Correspondence to:** Philip Känel; **email:** philip.kaenel@ime.fraunhofer.de
**Keywords:** aging, proteostasis, heat shock proteins, chaperone, locomotor activity
**Received:** September 13, 2021 **Accepted:** March 24, 2022 **Published:** April 8, 2022



## ABSTRACT

**Proteostasis reflects the well-balanced synthesis, trafficking and degradation of cellular proteins. This is a fundamental aspect of the dynamic cellular proteome, which integrates multiple signaling pathways, but it becomes increasingly error-prone during aging. Phosphatidylethanolamine-binding proteins (PEBPs) are highly conserved regulators of signaling networks and could therefore affect aging-related processes. To test this hypothesis, we expressed PEPBs in a heterologous context to determine their ectopic activity. We found that heterologous expression of the tobacco (*Nicotiana tabacum*) PEBP NtFT4 in *Drosophila melanogaster* significantly increased the lifespan of adult flies and reduced age-related locomotor decline. Similarly, overexpression of the Drosophila ortholog CG7054 increased longevity, whereas its suppression by RNA interference had the opposite effect. In tobacco, NtFT4 acts as a floral regulator by integrating environmental and intrinsic stimuli to promote the transition to reproductive growth. In Drosophila, NtFT4 engaged distinct targets related to proteostasis, such as HSP26. In older flies, it also prolonged *Hsp26* gene expression, which promotes longevity by maintaining protein integrity. In NtFT4-transgenic flies, we identified deregulated genes encoding proteases that may contribute to proteome stability at equilibrium. Our results demonstrate that the expression of NtFT4 influences multiple aspects of the proteome maintenance system via both physical interactions and transcriptional regulation, potentially explaining the aging-related phenotypes we observed.**

## INTRODUCTION

Aging is characterized by the progressive disruption of cellular functions due to the accumulation of damaged DNA and proteins, which leads to the loss of homeostasis. Several proteins and signaling pathways control cellular homeostasis, including phosphatidylethanolamine-binding proteins (PEBPs), which are found in both animals and plants. In mammals, there are two conserved PEBPs (PEBP1-like and PEBP4-like) that integrate multiple signaling pathways to regulate cell behavior [1–3]. PEBPs have not been associated directly with aging at the organism level, but the dysregulation of PEBP expression correlates with tissue and organ degeneration. For example, the two human PEBPs are associated with several age-related, degenerative diseases, including diabetic nephropathy, Alzheimer's disease, and various cancers [4–9]. *PEBP4* expression is tightly regulated in healthy tissues, whereas *PEBP1* (also known as Raf kinase inhibitory protein, RKIP) is ubiquitously expressed, and its activity is mainly regulated by PKC-mediated phosphorylation at S153. A role in lipid or phospholipid metabolism was proposed for these proteins based on their ability to bind phosphatidylethanolamine or phosphatidylcholine, but this aspect has received little attention following the discovery that the molecular basis of PEBP pathogenicity mostly reflects their ability to inhibit protein kinases [10].

Eight *Drosophila melanogaster* genes encode PEBP-like proteins that are structurally similar to human RKIP (*Pebp1*, *CG10298*, *CG7054*, *CG6180*, *CG17919*, *a5*, *CG17917* and *CG30060*; Supplementary Figure 1). Some are expressed preferentially in certain tissues (*Pebp1* in the midgut; *CG10298, CG17917* and *CG30060* in the testis; and *a5* in the adult head) whereas *CG7054*, *CG6180* and *CG17919* are expressed ubiquitously [11]. Pebp1 was recently shown to be important for the regenerative capacity of the intestinal stem cell (ISC) niche because its suppression led to accelerated ISC proliferation promoted by the loss of enterocytes, whose survival relies on *Pebp1* expression. Declining *Pebp1* expression, as also observed during aging, was accompanied by the loss of its ability to inhibit extracellular signal-regulated kinase (ERK) activity and the tight regulation of EGFR/ERK signaling [12]. In addition, PEBP-like proteins may control innate immunity but their molecular functions in Drosophila remain largely unclear [13–16].

Three distinct PEBP subclades have evolved in flowering plants, related to the floral regulators TERMINAL FLOWER 1 (TFL1), FLOWERING LOCUS T (FT), and MOTHER OF FT AND TFL1 (MFT), respectively [17]. The best characterized plant PEBPs are the TFL1-like and FT-like proteins, the latter being of particular interest due to their further functional diversification [18–23]. FT-like proteins with opposing roles during development are involved in the formation of storage organs, such as potato tubers, but also during the floral transition. In our experiments, we tested two tobacco PEBPs comprising a representative floral activator (NtFT4) and floral repressor (NtFT2) from the FT-like subclade [18]. Whereas the different functions of human PEBPs are associated with overtly distinct structures, single amino acid exchanges in plants are sufficient to convert a floral activator into a floral repressor [24]. The ability for such subtle differences to define functionality, and the consistent lack of the typical C-terminal helix, are unique properties of plant PEBPs [25, 26].

To investigate the functions of PEBPs in more detail, we undertook interspecies analysis and determined the molecular, cellular and organism-level effects of animal PEBPs expressed in Arabidopsis (*Arabidopsis thaliana*) and tobacco (*Nicotiana tabacum*) and plant PEBPs expressed in Drosophila. The functions of animal PEBPs in plants were assessed by investigating their interaction with canonical partners of FT-like proteins and by the overexpression of different PEBPs. We selected the best-characterized human PEBPs (*RKIP* and *hPEBP4*) and Drosophila PEBPs (*Pebp1* and *CG7054*) for the stable transformation of the two model plants and subsequent phenotypic analysis. In a reciprocal experiment, we used the Gal4 system to individually express two closely-related but functionally distinct plant PEBPs (*NtFT2* and *NtFT4*) as well as their closest Drosophila homolog (*CG7054*) in Drosophila. Although the expression of animal PEBPs in plants had no significant effect on flowering time, we were able to confirm molecular interactions with the anticipated endogenous binding partners. In contrast, the expression of plant PEBPs in Drosophila increased the adult fly lifespan by up to one third, whereas the silencing of the endogenous PEBP CG7054 reduced longevity. This observation correlates with the ability of NtFT4 to promote the expression of the small heat shock genes *Hsp26* and *Hsp27* in older flies and its ability to interact with the HSP26 protein. Thus, our results indicate that PEBPs extend the activity of the proteome maintenance system.

## RESULTS

### The expression of animal PEBPs in plants has no effect on floral transition or growth

The regulation of flowering time by FT-like proteins requires the binding of 14-3-3 scaffolding proteins to recruit specific bZIP transcription factors such as NtFD1 [18, 27]. We found that Drosophila CG7054 (which has the highest similarity to tobacco PEBPs) is also able to interact with tobacco 14-3-3 proteins and the transcription factor NtFD1 in *Nicotiana benthamiana* leaves, as revealed by bimolecular fluorescence complementation (BiFC) (Figure 1A, 1B). But despite these canonical interactions, the ubiquitous expression of CG7054 or other Drosophila or human PEBPs – PEBP1, a chimeric CG7054 carrying segments of NtFT4 (CG7054-DS, Supplementary Figure 2), RKIP and hPEBP4 – in Arabidopsis and tobacco had a negligible impact on flowering time (Figure 1C–1G).

We established stable transgenic lines expressing these PEBPs under the control of the strong cauliflower mosaic virus 35S promoter (35S) or the quadruple 35S promoter (Q35S) and selected independent lines with

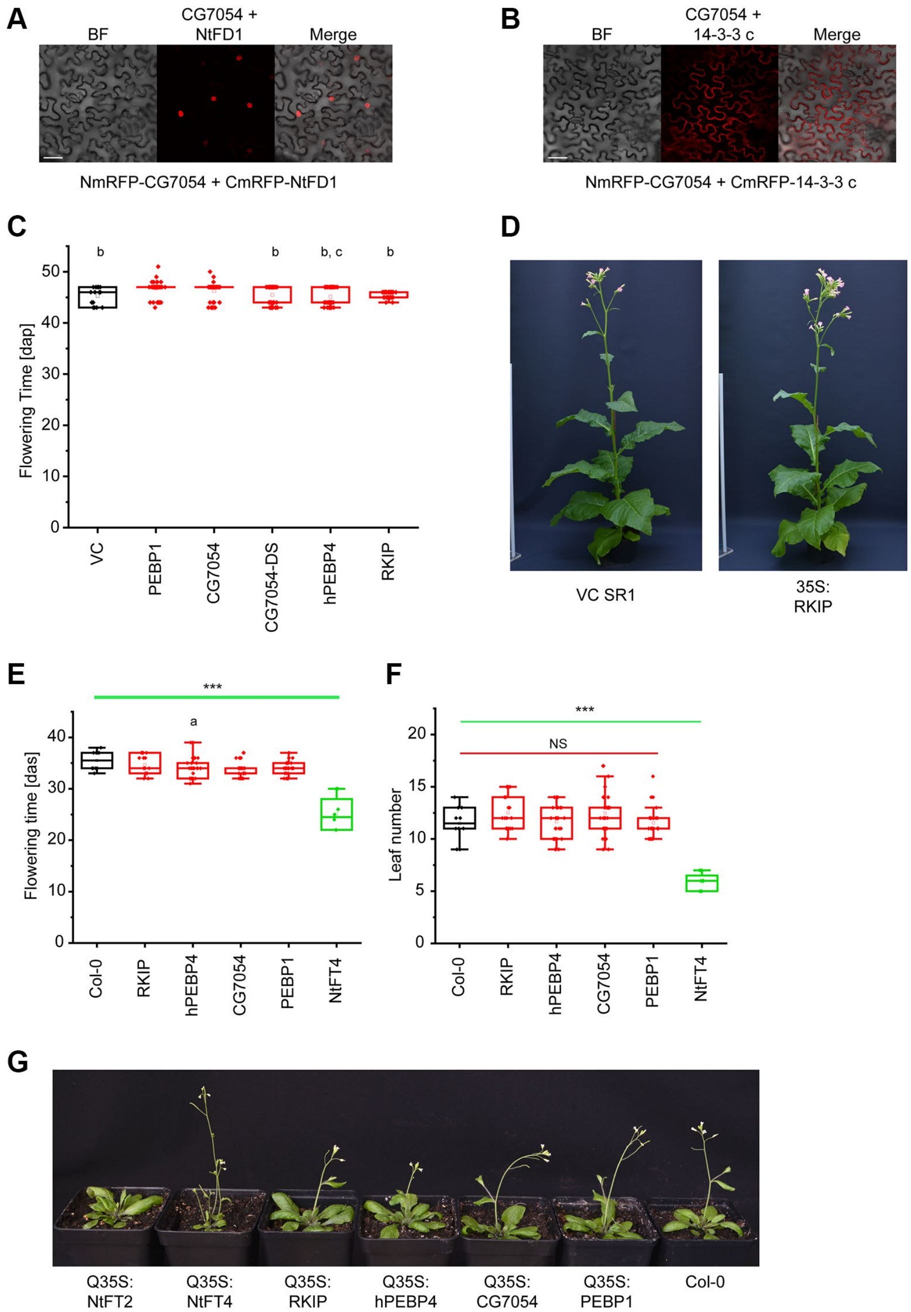


**Figure 1. Expression of animal PEBPs in tobacco and Arabidopsis.** (**A**) Bimolecular fluorescence complementation (BiFC) in infiltrated *Nicotiana benthamiana* leaves, representatively showing the interaction between Drosophila PEBP (NmRFP-CG7054) and NtFD1 (CmRFP-NtFD1). (**B**) BiFC representatively showing the interaction between Drosophila PEBP (NmRFP-CG7054) and tobacco 14-3-3 c (CmRFP-14-3-3 c). Scale bar = 50 µm. (**C**) Flowering time of tobacco lines expressing PEBP1, CG7054, CG7054-DS, RKIP or hPEBP4 under the control of the cauliflower mosaic virus 35S promoter. Abbreviation: VC: vector control. Flowering time was measured under long-day (LD) conditions in days after potting (dap). Data are means ± SEM, $n$ = 50 (PEBP1, CG7054, CG7054-DS, RKIP and hPEBP4), $n$ = 10 (VC). Significance was tested by one-way ANOVA and Tukey's *post hoc* test (*b* significant compared with PEBP1, *c* significant compared with CG7054, all other comparisons non-significant). (**D**) Representative image of a transgenic tobacco plant expressing RKIP compared with the VC. Flowering time (**E**) and rosette leaf number at the onset of flowering (**F**) of transgenic Arabidopsis lines expressing RKIP, hPEBP4, CG7054, PEBP1 or the floral inducer NtFT4 under the control of the quadruple cauliflower 35S promoter. Col-0 = wild type *A. thaliana* Col-0 ecotype used for transformation. Flowering time was measured under LD conditions in days after seeding (das). Data are means ± SEM, $n$ = 30 (CG7054, CG19594), $n$ = 29 (hPEBP4), $n$ = 19 (RKIP), $n$ = 10 (Col-0), $n$ = 8 (NtFT4); $^{****}p < 0.001$ in all pairwise comparisons with NtFT4 (*a* significant compared with Col-0 ($p$ = 0.091) with all other comparisons being non-significant). Abbreviation: *NS*: no significant differences in any pairwise comparison. All $p$-values are provided in Supplementary Table 9. (**G**) Representative images of transgenic Arabidopsis plants expressing different PEBPs. Col-0 wild type plants (far right), and early flowering Q35-S:NtFT4 (left) and late flowering Q35-S:NtFT2 (far left) plants are shown in comparison with plants expressing the animal PEBPs.

high PEBP expression levels for phenotyping. All tobacco plants expressing animal PEBPs flowered ~46 days after potting (dap), specifically hPEBP4 = 45.14 ± 0.24 dap and PEBP1 = 46.7 ± 0.20 dap, which was comparable to the vector control (45.3 ± 0.44 dap). The maximum delay was 1.4 days for PEBP1 (Figure 1C). In addition, ubiquitous expression of animal PEBPs did not cause any change in plant size or architecture (Figure 1D). In Arabidopsis, flowering times ranged from 32.7 ± 0.47 days after seeding (das) (hPEBP4) to 35.6 ± 0.57 das (RKIP) in lines expressing animal PEBPs, and were therefore comparable to the control (35.7 ± 0.61 das) and significantly later than flowering in the line expressing the floral activator NtFT4 (25.3 ± 0.61 das, Figure 1E).

The difference between animal and plant PEBPs was also very pronounced when comparing rosette leaf numbers at the onset of flowering (Figure 1F, 1G). NtFT4 expression significantly reduced the leaf number at this stage to 5.71 ± 0.29, whereas control plants (12.0 ± 0.62) and lines expressing animal PEBPs (PEBP4 = 11.71 ± 0.64, RKIP = 13.29 ± 0.61) had similar numbers of leaves. Some plants expressing the floral repressor NtFT2 did not flower by the end of the experiment (Figure 1G). Interaction with 14-3-3 proteins and the transcription factor FD therefore appears to be necessary, but not sufficient, for floral regulation.

**PEBPs increase the lifespan of Drosophila**

In the reciprocal experiment, we investigated the impact of expressing tobacco PEBPs (NtFT4 or NtFT2) or Drosophila CG7054 on fly morphogenesis and aging. We prepared UAS-based expression constructs and used the φC31 system for integration into the landing site 86Fb to ensure comparable expression levels for each transgene [28]. All constructs were constitutively expressed using the *daughterless-Gal4* system (*da-Gal4*). The specific role of Drosophila PEBPs in aging has not been reported before, so we also silenced the *CG7054* gene by RNA interference (RNAi) and investigated the physiological effects. Longevity was determined in groups of 20 mated females or males for all lines (lifespan data for male flies are provided in Supplementary Table 1). Among all the overexpression lines, the ubiquitous expression of NtFT4 showed the strongest effect on longevity (Table 1, Figure 2A), increasing the lifespan of female flies by 29.8% (median lifespan NtFT4♀ = 61 days, control♀ = 47 days). The expression of CG7054 or NtFT2 increased the lifespan by 14.9% (median lifespan CG7054♀ = 54 days, NtFT2♀ = 54 days; Table 1, Figure 2B, 2C). However, analysis of the first quartile (25% of the NtFT2 population) based on Kaplan-Meier survival curves revealed early mortality (NtFT2♀ = 44 days, control♀ = 47 days) whereas the opposite was observed for flies expressing CG7054 or NtFT4, where the first quartile survived longer than control flies (CG7054♀ = 54 days, NtFT4♀ = 56 days). CG7054 and NtFT4 therefore conferred a degree of longevity, but NtFT4 extended the lifespan significantly further than CG7054 (Table 1). The knockdown of *CG7054* in muscle cells using *Mef2-Gal4* was previously shown to cause late pupal lethality [29]. We used the *da-Gal4* system to achieve *CG7054* knockdown in all cells, which caused 40% of the animals to die during late pupal stages ($n$ = 748). The surviving adult flies expressing $CG7054^{dsRNA}$ had much shorter lifespans, reduced by 40.5% in males and 55.3% in females compared to controls (Figure 2D). In addition to the overall shorter lifespan, the knockdown of *CG7054* also caused approximately 20% of adult flies to die within two days (Table 1, Figure 2D).

**PEBPs increase locomotor activity of Drosophila**

Old flies expressing CG7054 or NtFT4 showed higher rates of motility than similarly-aged control flies. To quantify locomotion of adult flies we employed the rapid iterative negative geotaxis (RING) assay to characterize age-related decline in the locomotor ability of flies climbing the side of a tube [30]. Control female flies always show greater motility than age-matched males, so we tested the two sexes separately. We compared flies expressing NtFT4 (long-lived) or $CG7054^{dsRNA}$ (short-lived) to controls at different ages (10, 30 and 45 days) although the short lifespan of the $CG7054^{dsRNA}$ flies prevented the tests of this genotype at 45 days (Figure 3). Female $CG7054^{dsRNA}$ flies showed a consistent locomotor decline compared to controls and NtFT4 flies regardless of age (−40.25% and −38.86% at 10 days old, −30.16% and −47.50% at 30 days old, compared to control and NtFT4 flies, respectively; Figure 3A). Interestingly, $CG7054^{dsRNA}$ expression did not affect the locomotor activity of male flies, regardless of their age (Figure 3B). In contrast, the NtFT4 expression increased locomotor activity in male flies of all ages compared to controls (+36.09% at 10 days old, +97.37% at 30 days old, +105.68% at 45 days old; Figure 3B). In addition, male *da* > *NtFT4* flies were even more active at 45 days old than the control flies at 30 days old based on the velocity of negative geotaxis (NtFT4♂ 45 days = 2.54 mm/s, control♂ 30 days = 1.71 mm/s, $p = 7.32 \times 10^{-9}$). In young female flies, NtFT4 expression had no effect on locomotor activity, but it increased the locomotor activity of old females (+33.02% at 30 days old, +43.35% at 45 days old, compared to controls; Figure 3A). At this stage, old *da* > *NtFT4* females showed locomotion comparable to control flies 15 days younger (NtFT4♀ 45 days = 1.71 mm/s, control♀ 30 days = 1.92 mm/s, $p = 0.64$).

**Plant and animal PEBPs differ in stability and subcellular localization**

In Drosophila, the different PEBPs were expressed from the same genomic locus suggesting that variation in expression levels should not account for the observed differences. To evaluate protein stability as a factor, we transiently expressed the different PEBPs with a hemagglutinin (HA) tag in Drosophila S2 and human embryonic kidney (HEK) 293T cells and compared mRNA and protein levels. In both cell lines, the plant PEBPs were less abundant than their fruit fly counterparts, particularly when comparing NtFT4 and

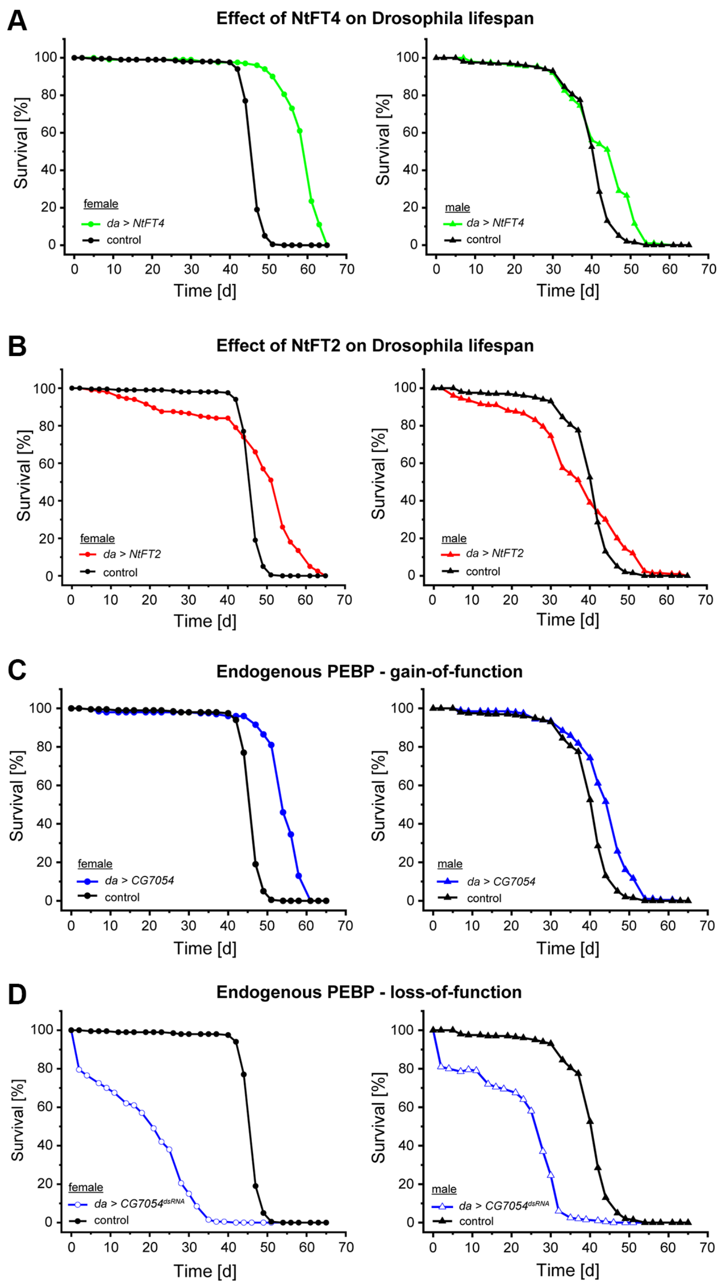


**Figure 2. Survival of Drosophila populations expressing NtFT4, NtFT2, CG7054 or CG7054$^{dsRNA}$ under the control of the *daughterless* (*da*) promoter**. Survival curves of female (left) and male (right) flies in the filial generation after mating *UAS-NtFT4*, *UAS-NtFT2*, *UAS-CG7054* or *UASt-CG7054$^{dsRNA}$* with the *da-Gal4* driver strain. (**A**, **B**) Effect on lifespan of flies constitutively expressing the floral inducer NtFT4 (**A**) or the floral repressor NtFT2 (**B**) compared with *da-Gal4* x Oregon-R ($n$ = 200). (**C**, **D**) Effect on lifespan of flies constitutively expressing the Drosophila PEBP *CG7054* (**C**) or constitutively silencing *CG7054* after mating *UASt-CG7054$^{dsRNA}$* with the *da-Gal4* driver strain (**D**) compared with *da-Gal4* x Oregon-R ($n$ = 200). Median and mean lifespans and statistical evaluation are summarized in Table 1 (female flies) and Supplementary Table 1 (male flies).

**Table 1. Survival of female flies with dysregulated PEBP expression ([*da-Gal4/UAS-CG7054*, *da-Gal4/UAS-NtFT2* or *da-Gal4/UAS-NtFT4*] or [*da-Gal4/UASt-CG7054$^{dsRNA}$*]) compared to +/*da-Gal4* controls.**

| | Median lifespan [d] | 25% Estimate [d] | Mean lifespan [d] | Equality vs. control ($\chi^2$) | Equality vs. CG7054 ($\chi^2$) | Equality vs. NtFT2 ($\chi^2$) |
|---|---|---|---|---|---|---|
| **Control** | 47 | 47 | 46.19 (± 0.34) | – | – | – |
| **CG7054** | 54 | 54 | 54.00 (± 0.57) | 313.72 ($p$ = 0) | – | – |
| **CG7054$^{dsRNA}$** | 21 | 7 | 18.91 (± 0.83) | 447.62 ($p$ = 0) | 440.96 ($p$ = 0) | – |
| **NtFT2** | 54 | 44 | 47.66 (± 0.97) | 94.87 ($p$ = 0) | 14.02 ($p = 1.81 \times 10^{-4}$) | – |
| **NTFT4** | 61 | 56 | 58.50 (± 0.51) | 371.28 ($p$ = 0) | 110.56 ($p$ = 0) | 119.98 ($p$ = 0) |

Median lifespans, 25% quartile estimates and mean lifespans were calculated based on Kaplan-Meier survival curves and $\chi^2$ and $p$-values were calculated using the Mantel-Cox method.

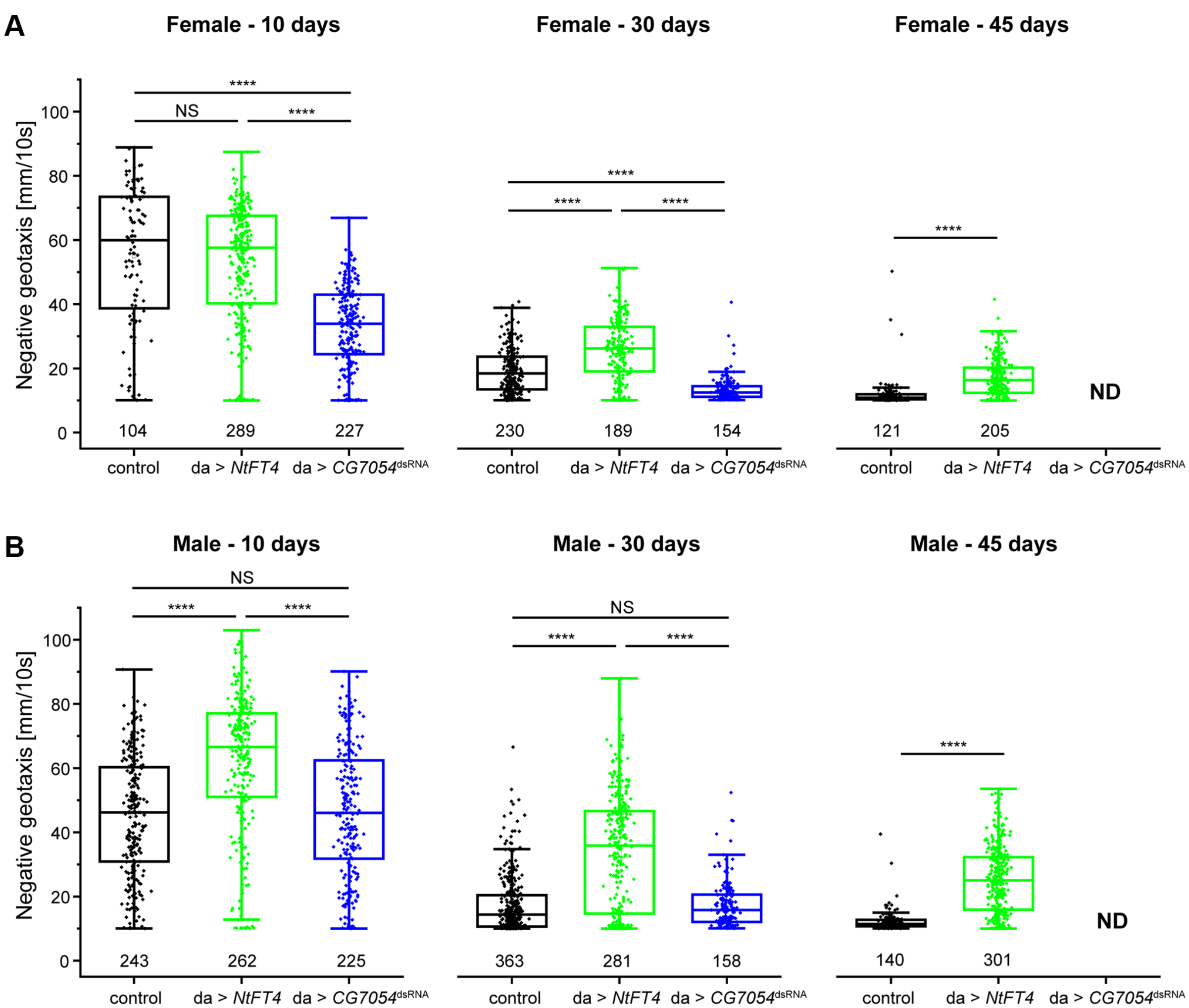


**Figure 3. Locomotor behavior of long-lived (*da > NtFT4*) or short-lived (*da > CG7054$^{dsRNA}$*) Drosophila populations at different ages.** Rapid iterative negative geotaxis (RING) assay with virgin female (**A**) and male (**B**) flies at 10, 30 or 45 days old. The locomotor behavior was analyzed in the filial generation after mating Oregon-R (control, black), *UAS-NtFT4* (green) or *UASt-CG7054$^{dsRNA}$* (blue) flies with the *da-Gal4* driver strain. Negative geotaxis was plotted as average velocity (mm/10 s) and was traced for all tracks traveled in the population (numbers below plots). Significance was tested by one-way ANOVA and Tukey's *post hoc* test between control, *da > NtFT4* and *da > CG7054$^{dsRNA}$* ($^{****}p < 0.001$, Abbreviation: *NS*: not significant). All $p$-values are provided in Supplementary Table 9.

CG7054 (Supplementary Figure 3). Although *HA-NtFT4* and *HA-CG7054* mRNA were expressed at comparable levels, only HA-CG7054 was detected in the protein extracts (Supplementary Figure 3A). Green fluorescent protein fusions of the tobacco FT-like proteins (HA-EGFP-NtFT4 and HA-EGFP-NtFT2) appeared more stable than HA-NtFT4 and HA-NtFT2 (Supplementary Figure 3B). As shown above for the HA-tagged constructs, the HA-EGFP-CG7054 protein accumulated to higher levels than HA-EGFP-NtFT4, although *HA-EGFP-NtFT4* mRNA was more abundant than *HA-EGFP-CG7054* mRNA (19.03 ± 1.5 vs. 5.95 ± 0.25; Supplementary Figure 3C). These data suggest there is no correlation between longevity and the abundance of PEBPs.

Interestingly, whereas the fly PEBPs CG7054, PEBP1 and CG10298 were uniformly located in all cellular compartments in HEK-293T and S2 cells, NtFT4 and NtFT2 were enriched in nuclear speckles (Supplementary Figure 3D). The distinctive nuclear localization of NtFT4 and NtFT2 was also found for HA-tagged NtFT proteins in Drosophila fat body cells (Supplementary Figure 3E). The distinct subcellular localization of NtFT4 and NtFT2 compared to CG7054 and PEBP1 may indicate a specific function in the nucleus. The NtFT2 and NtFT4 peptide sequences do not contain a nuclear localization signal to explain their accumulation (Supplementary Figure 4A). In plants, FT-like proteins translocate to the nucleus when they interact with FD-like bZIP transcription factors, and a similar mechanism may therefore operate in Drosophila cells.

**The NtFT4 interactome reflects its multifunctional role**

To determine how NtFT4 affects longevity, we set out to identify its interaction partners in Drosophila using a yeast two-hybrid (Y2H) library and mass spectrometry following co-immunoprecipitation from extracts of transiently transfected S2 cells expressing HA-EGFP-tagged NtFT4. In the former case, we used a Drosophila normalized cDNA library to ensure the detection of rare interactions. Because the NtFT4 fusion with the DNA-binding domain of Gal4 (Gal4$^{BD}$) caused auto-activation, we used the related NtFT2 protein as the initial bait. NtFT2 and NtFT4 share 70.2% amino acid sequence identity and they have similar predicted structures (Supplementary Figure 4B–4D). Moreover, NtFT2 overexpression increases longevity to the same extent as CG7054 (Table 1). We isolated 72 colonies from the cDNA library on selective medium. Sequencing and subsequent cloning of the full coding sequences followed by re-analysis in a drop test confirmed interactions between NtFT2 and nine Drosophila proteins (Supplementary Figure 5A). The interactions with CG6523, CG7220, CKIIα-i3, mRpL44, RHEB and YIPPEE were confirmed using BiFC assays (Supplementary Figure 5B), whereas the interactions with ACT42A, CG31644 and 4E-T remain uncertain because they were not verified in the Y2H drop test (ACT24A) or by BiFC (CG31644, 4E-T). The unconfirmed interactions in Y2H drop tests are shown in Supplementary Figure 6. Further BiFC experiments revealed that six of these initial candidates (ACT42A, CG6523, CG7220, CKIIα-i3, mRpL44 and RHEB) also interact with NtFT4 and CG7054. Interestingly, the YIPPEE protein was shown to interact with NtFT2 and CG7054 but not with NtFT4 (Supplementary Figure 5B).

To refine the list of interaction partners in a Drosophila cell model, we performed immunoprecipitation experiments using transiently transfected S2 cells expressing NtFT4 tagged with HA-EGFP (at the C-terminus or N-terminus) and used HA-EGFP as a reference. We were unable to detect HA-tagged NtFT4 in extracts of the transgenic flies, thus preventing *in vivo* interaction assays. The precipitates generated using HA-EGFP and HA-EGFP-NtFT4 (Supplementary Figure 7) were analyzed by LC-MS/MS. This revealed 23 putative NtFT4 interaction partners (Supplementary Table 2). Following the cell model, we confirmed the interactions between NtFT4 and CCT7, CG4364, HSP26, PEN, PyK and TSN by co-immunoprecipitation (Figure 4A) and fluorescence resonance energy transfer (FRET) analysis (Figure 4B). The gating strategy to quantify FRET efficiency in all experiments is shown in Supplementary Figure 8. Although we detected a FRET signal when CG7054 was combined with HSP26, PEN and TSN, these interactions were inconclusive and significantly weaker than the corresponding assays with NtFT4. EYFP-HSP26 achieved the following FRET efficiencies: CER-NtFT4 = 13.8%, CER-CG7054 = 2.3% and CER = 0.78%. When testing EYFP-PEN, the equivalent results were CER-NtFT4 = 7.9%, CER-CG7054 = 0.5% and CER = 0.2%. Finally with EYFP-TSN, the results were CER-NtFT4 = 3.8%, CER-CG7054 = 0.4% and CER = 0.0% (Figure 4B). There was no overlap between the interactions detected in the *in vivo* Y2H assay and those based on protein complexes extracted from Drosophila S2 cells.

According to Flybase and the String database [31, 32], the NtFT4 interaction partners in Drosophila include proteins associated with chaperone-mediated protein folding (CCT2, CCT7 and HSP26), protein ubiquitination (CG7220) and phosphorylation (RHEB and PEN), stress responses (CG7220, RHEB, HSP26 and TSN) and longevity (HSP26, RHEB and PyK) (Supplementary Figure 9). The results for RHEB and

PyK revealed only indirect links to longevity via their interaction network (RHEB; Supplementary Figure 9) or an ortholog (Pyk in *Caenorhabditis elegans*) [33]. However, there is direct evidence that the small heat shock protein family is sufficient to promote longevity in flies [34]. Furthermore, the interaction between NtFT4 and HSP26 is highly conspicuous given the strength of the interaction suggested by FRET and

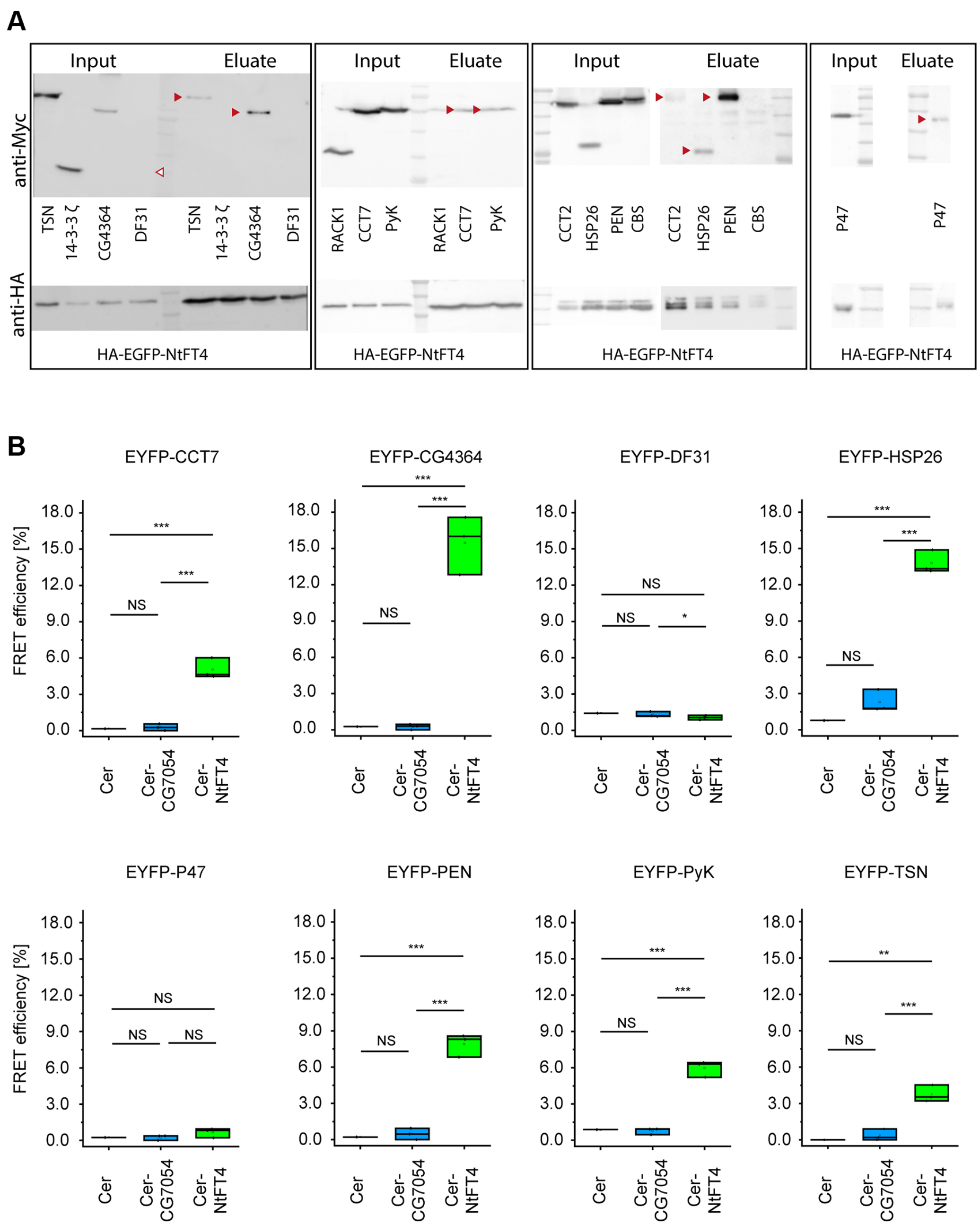


**Figure 4. Interaction partners of NtFT4 identified in immunoprecipitated protein complexes after transient expression in S2 cells.** The abundance of the interaction partners was confirmed by immunodetection using mouse anti-Myc (top) or rabbit anti-HA (bottom) antibodies in the extracts and successful precipitation with magnetic anti HA-beads was confirmed by the detection of HA-EGFP-NtFT4 in the eluates. (**A**) Western blots of extracts (Input) and eluates after co-immunoprecipitation (Eluate) following transient co-transfection of S2 cells with HA-EGFP-NtFT4 plus Myc-Tsn, Myc-14-3-3 ζ, Myc-CG4364, Myc-Df31, Myc-Rack1, Myc-CCT7, Myc-PyK, Myc-CCT2, Myc-Hsp26, Myc-Pen, Myc-Cbs or Myc-p47. Detection of co-immunoprecipitated proteins in the eluate is indicated by red arrowheads. Df31 was not detected in extracts under the mild conditions used for immunoprecipitation (empty arrowhead). (**B**) Analysis of FRET efficiency in co-transfected cells expressing the donors Cerulean (Cer, negative control), Cer-NtFT4 or Cer-CG7054 plus the acceptors EYFP-CCT7, EYFP-CG4364, EYFP-Df31, EYFP-Hsp26, EXFP-p47, EYFP-Pen, EYFP-PyK or EYFP-Tsn by flow cytometry. Gating strategy and representative controls are shown in Supplementary Figure 8. Cer-NtFT4 and Cer-CG7054 were co-transfected in three independent triplicates ($n$ = 3) and statistical significance was tested by one-sample $t$-test ($^{****}p < 0.001$, $^{***}p < 0.01$, $^{**}p < 0.05$, $^{*}p < 0.1$, Abbreviation: *NS*: not significant).

co-immunoprecipitations experiments (Figure 4, Supplementary Figure 10). We therefore investigated the relationship between HSP26 and NtFT4 in more detail.

**NtFT4 interacts with HSP26 and stabilizes its expression in older flies**

Heat shock proteins are often induced by stress, particularly heat stress. We observed no significant upregulation of any heat shock gene following transfection with *NtFT4* or any other construct (Figure 5A, 5B). However, we detected significant increases in the expression of *Hsp22*, *Hsp23*, *Hsp26*, *Hsp27* and *Hsp70Aa* under heat stress, regardless of transfection. We also confirmed the accumulation of HSP26 protein in response to heat stress but not transfection (Figure 5C). Neither transfection nor heat shock affected the expression of *HspB8*, *l(2)efl* or *Hsc70–4*. These data suggest that NtFT4 expression *per se* does not elicit a stress response.

The expression of *Hsp26* and *Hsp27* decreases as flies age [35]. Accordingly, we quantified the expression of different heat shock family members at different ages in flies, revealing that NtFT4 significantly enhances the expression of *Hsp26* and *Hsp27,* which encode the most abundant members of the small heat shock protein family (Figure 6A–6D). In contrast, NtFT4 did not affect the expression of *Hsp83* and *Hsc70–4*, which encode the most abundant larger heat shock proteins (Figure 6C). No consistent correlation between NtFT4 and the expression of genes encoding other small (*Hsp22* and *Hsp23*) or larger (*HspB8, Hsc70–3, DnaJ-1, l(2)efl, Hsp68* and *Hsp70Aa*) heat shock proteins was observed, emphasizing the specific link between NtFT4 and *Hsp26* and *Hsp27*. The expression of *Hsp26* was mirrored by the abundance of HSP26 protein, which decreased stepwise in control flies aged 20+ days, eventually becoming barely detectable after 50 days (Figure 6E, 6F). The abundance of HSP26 also decreased with age in flies expressing NtFT4, but the rate of decline was shallower and the protein was still detectable in flies aged 50 d, comparable to the levels at 30 d in control flies (Figure 6E).

**NtFT4 induces differential gene expression related to metabolism and proteostasis**

The nuclear localization of plant PEBPs in Drosophila cells suggests that their effect on longevity may reflect their ability to regulate transcription or mRNA metabolism. Genome-wide transcriptome analysis was therefore carried out to identify dysregulated genes using the Affymetrix GeneChip Drosophila Genome 2.0 array. We used female flies due to their pronounced longevity phenotype. Overall, we observed a high correlation in gene expression between control flies and those expressing NtFT4, as shown by correlation coefficients ranging from 0.973 to 0.997 (Supplementary Table 3). We detected 49 genes with significant upregulation and 100 with significant downregulation, defined as a fold change of at least 1.5 with a *p*-value less than 0.05 (Supplementary Table 4).

The low number of modulated genes facilitated the subsequent verification of differentially expressed genes as well as functional enrichment analysis. The expression of NtFT4 mainly affected genes involved in metabolic processes (Supplementary Tables 5 and 6), specifically 27.8% of the modulated genes were assigned to the protein class *metabolite interconversion enzyme* and 9.3% to the class *protein modifying enzyme* (Figure 7A, Supplementary Table 6). In the latter, eight of the nine identified gene products were annotated as proteases and four others (Jon66Ci, CG31205, CG11841 and CG42694) were putative proteases containing peptidase sequence motifs (Table 2). We also found four uncharacterized proteins that may function as protease inhibitors or regulators of proteolysis (the serpins Spn47C and Spn43Ab, and the Kazal-domain proteins Kaz1-ORFB and CG1077).

Quantitative RT-PCR analysis confirmed the differential expression of genes encoding the predicted proteases CG1304, CG31205, CG31681, CG32277, CG32523, Jon66Ci and Ser6, and the serpin Spn47C (Figure 7B). We also confirmed the differential expression of genes involved in metabolic processes. The significantly downregulated genes in flies expressing NtFT4 included *Cyp6a17*, *Fad2*, *CG17322*, *CG18609*, *α-Est10* and *GstE5*, whereas *CG15661*, *CG4302*, *CG15334*, *CG7900*, *GstD1* and *GstD5* were significantly upregulated (Figure 7C). We also confirmed the differential expression of *CG14406*, *CG14410*, *CG15570*, *CG12057*, *sei* and *tkv* (upregulated), as well as *CG16898*, *CG17478*, *l(2)03659*, *CG42825*, *CG11825*, *CG30272* and *CG13422* (downregulated), which either await functional characterization or cannot be grouped according to their functions (Figure 7D).

We also looked at direct molecular markers of aging. Protein carbonylation results from oxidative damage that accumulates with age. Given the numerous differentially expressed genes and interacting proteins involved in proteostasis, we also tested whether long-lived flies expressing NtFT4 or CG7054 had lower protein carbonylation levels. However, there were no significant differences in protein carbonylation when comparing either *NtFT4* or *CG7054* expressing flies to controls at 10 or 30 days old (Supplementary Figure 11).

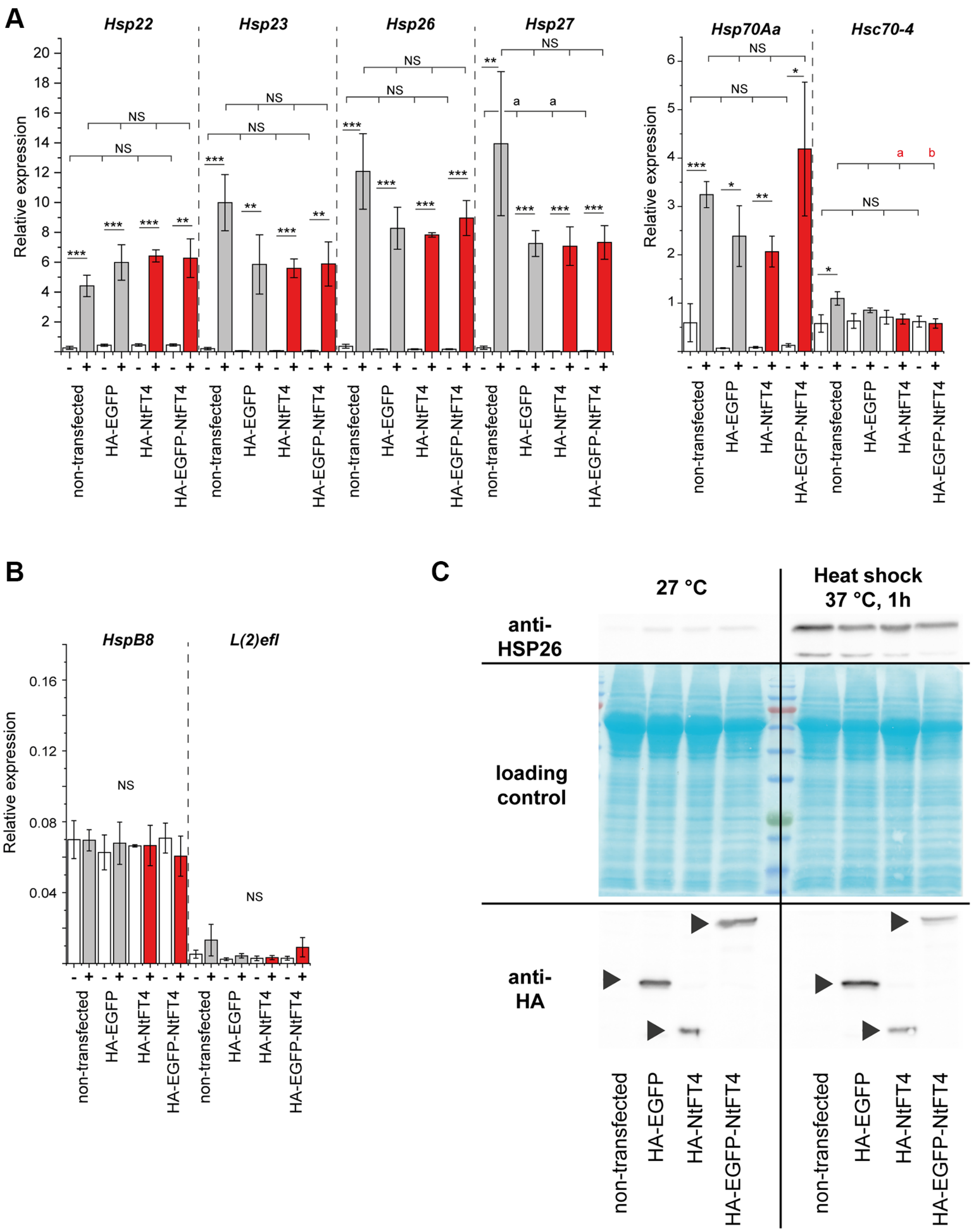


**Figure 5. Transfection and heat stress response of heat shock proteins in S2 cells.** Expression of stress-responsive (*Hsp22, Hsp23, Hsp26, Hsp27, Hsp70Aa* and *Hsc70–4*) (**A**) and non-responsive (*HspB8* and *l(2)efl*) (**B**) heat shock protein genes in S2 cells after transient transfection with HA-EGFP, HA-NtFT4 or HA-EGFP-NtFT4 compared to non-transfected cells. After transfection and induction of gene expression, cells were cultivated at 27°C (–, white bars) or stressed by heat shock at 37°C for 1 h (+, gray bars show controls and red bars show NtFT4). Relative gene expression was analyzed by qRT-PCR using *Gapdh2* as a reference. Data are means ± SEM ($n$ = 3). Significance was tested by one-way ANOVA and Tukey's *post hoc* test for responses to transfection (untransfected vs. HA-EGFP vs. HA-NtFT4 vs. HA-EGFP-NtFT4; $a$ = significant compared to nontransfected cells, $p < 0.1$; $b$ = significant compared to nontransfected cells, $p < 0.05$; Abbreviation: *NS*: not significant including all remaining comparisons) and using a $t$-test for pairwise comparisons of individual responses to heat shock ($^{****}p < 0.001$, $^{***}p < 0.01$, $^{**}p < 0.05$, $^{*}p < 0.1$, Abbreviation: *NS*: not significant). (**C**) Immunodetection of HSP26 following the transient transfection of S2 cells with HA-EGFP, HA-NtFT4 or HA-EGFP-NtFT4 compared with nontransfected cells. The response of HSP26 to transfection and to heat shock at 37°C was analyzed 1 h after treatment by extracting proteins for immunodetection using anti-HSP26 antibodies (top right). The transient expression of HA-EGFP, HA-NtFT4 or HA-EGFP-NtFT4 was confirmed using anti-HA antibodies (bottom, arrowheads). All $p$-values are provided in Supplementary Table 9.

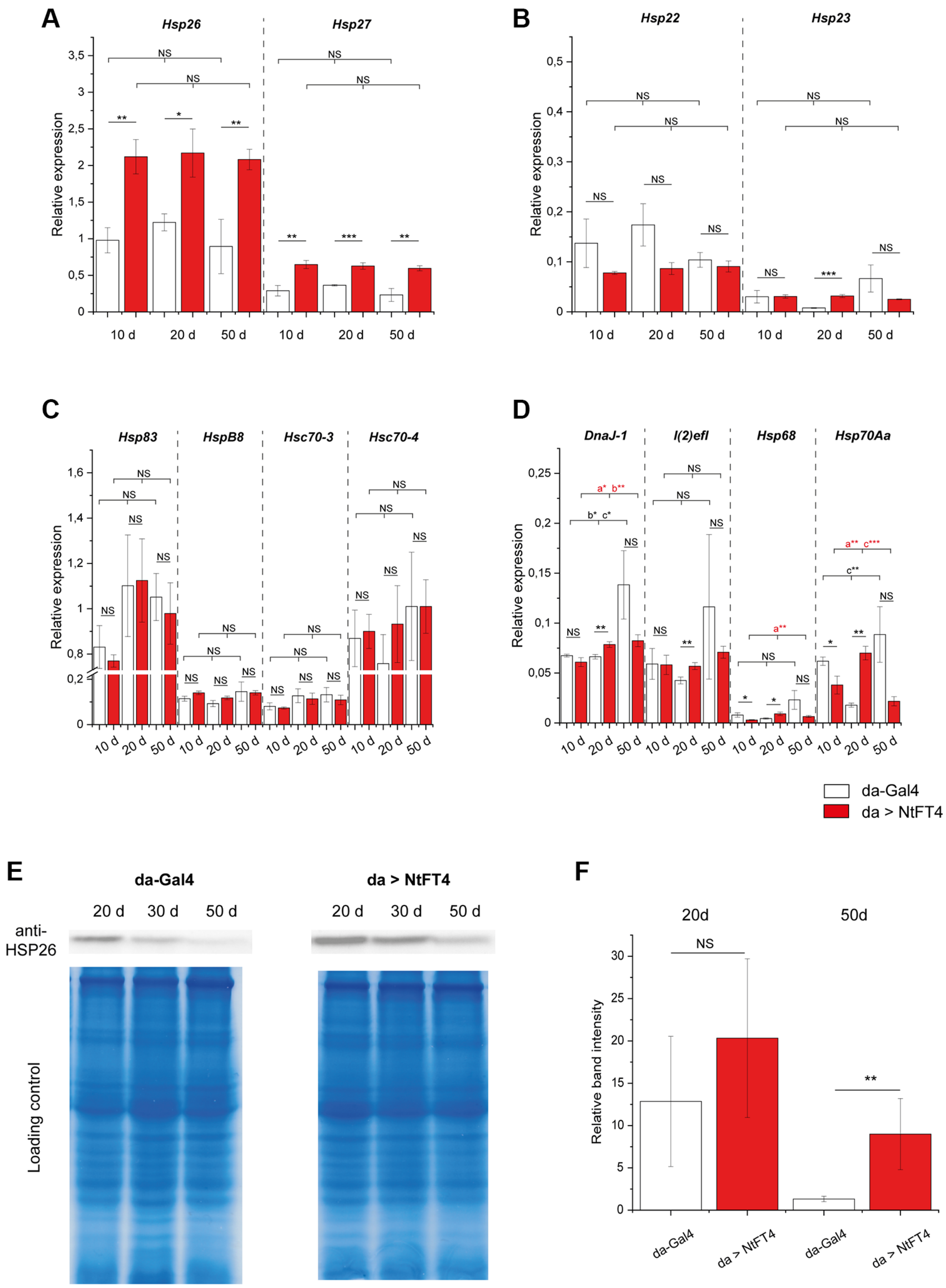


**Figure 6. Expression of heat shock genes during aging in flies expressing NtFT4.** Relative expression of two small heat shock protein genes directly associated with aging (*Hsp26* and *Hsp27*) (**A**), of the two small heat shock protein genes *Hsp22* and *Hsp23* (**B**), of larger heat shock protein genes *Hsp83*, *HspB8*, *Hsc70-3* and *Hsc70-4* (**C**), and of weakly-expressed heat shock protein genes *DnaJ-1*, *l(2)efl*, *Hsp68* and *Hsp70Aa* (**D**) in female *da > NtFT4* flies aged 10, 20 and 50 d, compared with *da-Gal4* flies by quantitative RT-PCR. Relative expression was calculated using *Gapdh2* as a reference gene. Data are means ± SEM ($n$ = 3). Significance was tested by one-way ANOVA and Tukey's *post hoc* test for changes during age (10 d vs. 20 d vs. 50 d) and using a $t$-test for pairwise comparisons between *da-Gal4* and *da > NtFT4* flies ($^{***}p < 0.01$, $^{**}p < 0.05$, $^{*}p < 0.1$, Abbreviation: *NS*: not significant; $a$ = significant between 10 d and 20 d, $b$ = significant between 10 d and 50 d, $c$ = significant compared between 20 d and 50 d). (**E**) Western blot showing the detection of HSP26 in protein extracts from female *da > NtFT4* flies aged 10, 20 and 50 d, compared with *da-Gal4* flies. A representative Western blot is shown for anti-HSP26 and comparable protein loading was ensured by staining with Coomassie Brilliant Blue. (**F**) Quantification of relative band intensities from three independent Western blot samples from 20 d (highest levels of HSP26 protein) and 50 d old flies. The relative band intensity was measured with imageJ and calculated by referring to the weakest band on each blot (50 d old *da-Gal4* flies). Data are means ± SEM ($n$ = 3), $p$ = 0.029 ($t$-test), Abbreviation: *NS*: not significant. The $p$-values of all comparisons are provided in Supplementary Table 9.

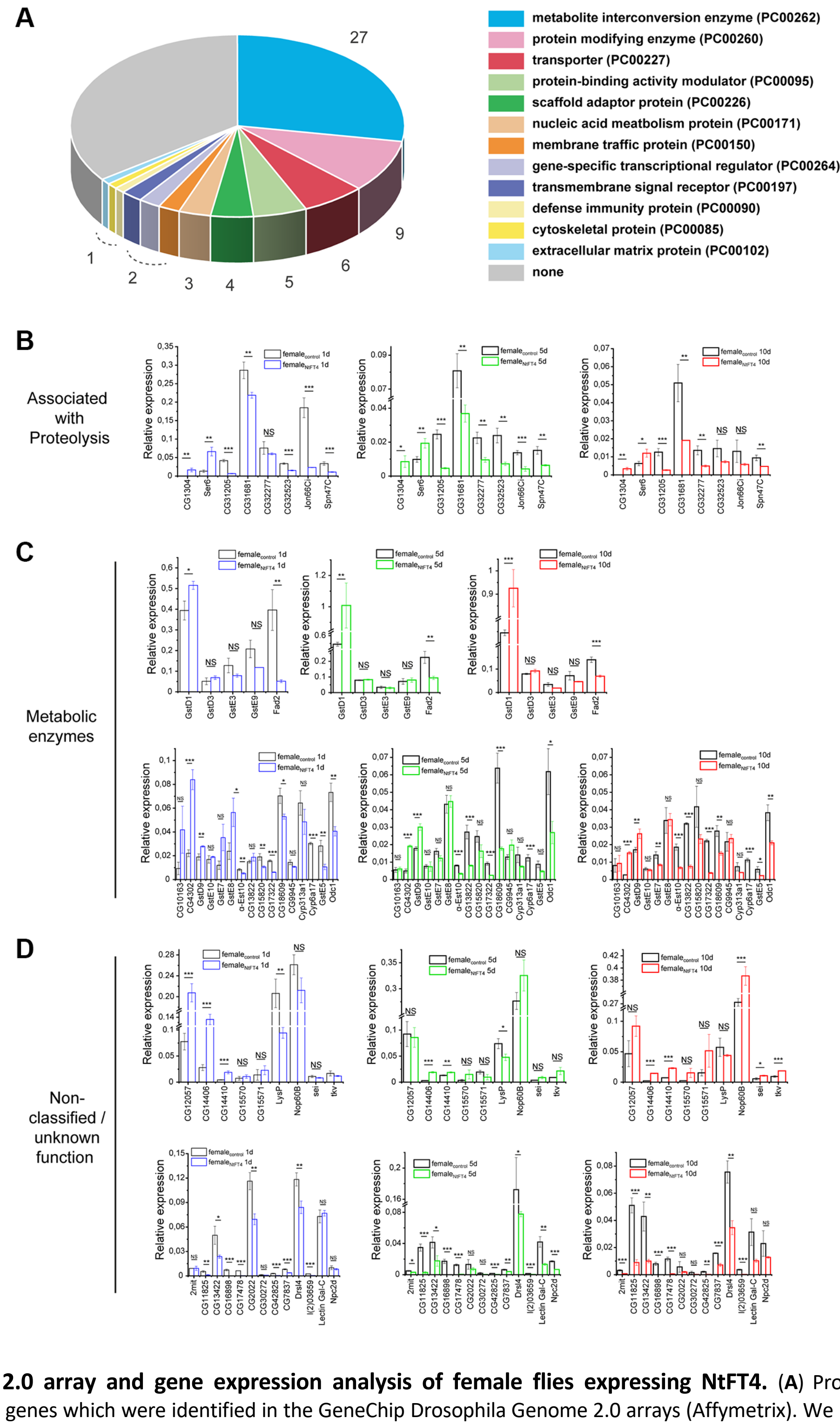


**Figure 7. GeneChip 2.0 array and gene expression analysis of female flies expressing NtFT4.** (**A**) Protein classes encoded by differentially expressed genes which were identified in the GeneChip Drosophila Genome 2.0 arrays (Affymetrix). We identified 149 genes that were significantly deregulated in female flies expressing NtFT4, 97 of which were mapped in the Panther database, and 63 genes were classified as representing 12 different protein classes. The largest protein classes were PC00262 (metabolite interconversion enzymes, 27 genes) and PC 00260 (protein modifying enzymes, 9 genes). Significance was determined using the paired *t*-test. Deregulated genes were included with a $\log_2$ fold change > 1.5 and a *p*-value < 0.05, *n* = 3. (**B**–**D**) Gene expression analysis. Deregulated genes associated with proteolysis (*CG1304*, *Ser6*, *CG31205*, *CG31681*, *CG32277*, *CG32523*, *Jon66Ci* and *Spn47C*) (**B**), annotated as *metabolic enzymes* (**C**), or genes which cannot be classified into groups and genes of unknown function (*non-classified/unknown function*) (**D**) identified by transcriptome analysis were analyzed individually in 1d (left, blue), 5 d (middle, green) or 10 d (right, red) old female flies expressing NtFT4 (*da > NtFT4*) compared with control (*da-Gal4*) flies (black). Relative expression levels were calculated in relation to the reference genes *Gapdh2*, *14-3-3 ε* and *RpL32*. Data are means ± SEM (*n* = 3), *p*-values are based on a *t*-test of pairwise comparisons between *da > NtFT4* and *da-Gal4* flies, $^{****}p$ < 0.001, $^{***}p$ < 0.01, $^{**}p$ < 0.05, $^{*}p$ < 0.1, Abbreviation: *NS*: not significant. The *p*-values of all comparisons are provided in Supplementary Table 9.

**Table 2. Genes encoding proteases or their inhibitors that are deregulated in female flies expressing *NtFT4*.**

| UniProtKB | Mapped IDs | Gene group (Flybase) | Symbol | FC | *p*-value |
|---|---|---|---|---|---|
| Q8IN51 | NM_169915 | S1A non-peptidase homolog | *CG31205* | −4.27 | $1.33 \times 10^{-2}$ |
| Q9VSJ1 | NM_168271 | S1A Serine proteases - Elastase-like | *Jon66Ci* | −3.90 | $9.50 \times 10^{-4}$ |
| Q8IPY7 | NM_164473 | S1A Serine proteases - Trypsin-like | *CG31681* | −2.26 | $4.05 \times 10^{-3}$ |
| Q8IQ51 | NM_167738 | S1A Serine proteases - Trypsin-like | *CG32523* | −2.26 | $1.16 \times 10^{-2}$ |
| Q8IRE1 | NM_168002 | S1A Serine proteases - Trypsin-like | *CG32277* | −2.03 | $4.72 \times 10^{-2}$ |
| Q9VAQ4 | NM_143404 | S1A Serine proteases - Trypsin-like | *CG11841* | −1.93 | $3.48 \times 10^{-2}$ |
| Q9VQA0 | NM_134818 | S1A Serine proteases - Trypsin-like | *Send1* | −1.67 | $3.72 \times 10^{-2}$ |
| Q9VAS2 | NM_143386 | Neprilysin-like metalloendopeptidase | *CG14528* | −1.63 | $2.77 \times 10^{-2}$ |
| A0A0B4JD89 | NM_001202065 | S1A non-peptidase homolog | *CG42694* | −1.61 | $1.79 \times 10^{-2}$ |
| Q9VRD1 | NM_134574 | S1A Serine proteases - Elastase-like | *CG1304* | 3.02 | $9.10 \times 10^{-3}$ |
| Q9VRD0 | NM_078702 | S1A Serine proteases - Elastase-like | *Ser6* | 2.00 | $4.28 \times 10^{-2}$ |
| Q9VMM2 | NM_135117 | Dipeptidyl peptidases IV | *CG11034* | 1.97 | $2.07 \times 10^{-2}$ |
| Q7K508 | NM_001169645 | Putative non-inhibitory serpin | *Spn47C* | −2.10 | $1.42 \times 10^{-2}$ |
| A1Z6V5 | NM_001032224 | Putative non-inhibitory serpin | *Spn43Ab* | −1.66 | $1.85 \times 10^{-2}$ |
| Q9VNL6 | NM_141360 | Kazal domain superfamily | *CG1077* | 4.70 | $2.79 \times 10^{-2}$ |
| O97042 | NM_001031920 | Kazal domain superfamily | *Kaz1-ORFB* | −1.55 | $2.62 \times 10^{-2}$ |

GeneChip Drosophila Genome 2.0 arrays (Affymetrix) revealed several deregulated proteases, protease inhibitors and uncharacterized proteins associated with proteolysis or its regulation [36, 37]. Fold-changes were calculated in comparison with *da-Gal4* flies and *p*-values were calculated using parametric *t*-tests.

## DISCUSSION

We investigated the activity of animal PEBPs expressed in Arabidopsis and tobacco, and of tobacco PEBPs expressed in Drosophila and human cells, as well as transgenic flies. The heterologous expression of the plant PEBPs (NtFT4 and NtFT2) in Drosophila resulted in a significant increase in longevity. In contrast, the expression of several animal PEBPs in plants had no significant effect on growth or development, including the floral transition. Although the animal PEBPs interacted with canonical partners of FT-like proteins in plants, the interactions with NtFD1 and 14-3-3 proteins were not sufficient to overcome endogenous regulatory cues controlling developmental transition. The nonreciprocal activity of plant and animal PEBPs may reflect differences in protein stability, subcellular localization or interaction partners [27].

Drosophila PEBPs are structurally similar to human PEBP1 (RKIP) and the crystal structure of CG7054 has been solved [38]. The structures share a short helical region at the C-terminus which is entirely missing from all plant PEBPs (Supplementary Figure 4). Instead, the C-terminal region of plant FT-like proteins features a protease cleavage site, which allows posttranslational modification [39]. The presence of this cleavage site could reduce the stability of heterologous plant PEBPs in animal cells and may contribute to the low NtFT protein levels we detected.

The known functions of PEBPs include the regulation of developmental transitions in plants and the regulation of cell survival, proliferation and differentiation in mammals [1–3, 17, 18, 20, 40]. The heterologous expression of NtFT4 in flies revealed new aspects of PEBP activity that point to a role in proteostasis, improving health and lifespan [41]. Mammalian and Drosophila PEBPs can interfere with protein kinase activity [4, 12, 42]. In humans, the inhibition of kinase signaling by RKIP depends on phosphorylation, which facilitates interactions with target kinases [1, 43–45].

Drosophila PEBPs are associated with fitness through their role in innate immunity, which is evidenced by the upregulation of PEBP genes during infections [13, 14] and the protection against bacterial infections conferred by the overexpression of *PEBP1* [16]. Our data provide additional links between PEBPs and fitness by demonstrating their impact on longevity and motility. First, we found that the ubiquitous knockdown of *CG7054* expression causes late pupal lethality in ~40% of the animals. Similarly, the knockdown of *CG7054* or *a5* was shown to be partly lethal in genome-wide RNAi experiments [29, 46]. As part of a systemic approach to assess muscle morphogenesis, the lethal effect of *CG7054* knockdown has been demonstrated at the late pupal stage when using the muscle-specific driver *Mef2-Gal4* [29, 47]. In addition to partial lethality, we demonstrated that the surviving adult flies showed reduced locomotor activity and the adult lifespan was significantly shorter. This complements our finding that the overexpression of either *CG7054* or *NtFT4* increases the longevity of flies. The expression of *NtFT4* not only increases the lifespan of flies but also counteracts age-related deterioration in locomotor behavior, one of the most serious behavioral disorders in old age [48]. Here we noted an interesting sex difference. Whereas *NtFT4* expression did not improve the locomotor abilities of young females, there were significant benefits in males and older females. There appears to be a maximum level of activity that cannot be improved in young female flies. In contrast, young males are generally less motile than young females but their locomotor activity is significantly enhanced by PEBP expression.

Some components of the NtFT4 interactome in Drosophila are already known to be associated with longevity, including PyK, RHEB and HSP26 [33, 34, 49, 50–53]. PyK and RHEB regulate mTOR kinase activity [49, 54, 55], thus the interaction with NtFT4 resembles the canonical regulatory mechanism of PEBPs. A link with the insulin/IGF and TOR signaling pathway (IIS/TOR), which also connects metabolism with cellular homeostasis and aging [56–58], is also supported by the interaction between NtFT4 and CCT7 (or other chaperonin-containing TCP1 subunits) [55]. CCTs are also targets of phosphorylation by RSK or S6K, downstream of mTOR activation by insulin [59]. The interactions with PyK, RHEB and CCTs may therefore integrate NtFT4 into the signaling network that controls longevity (Supplementary Figure 12).

The interaction between NtFT4 and HSP26 reveals a new mechanism of PEBP activity. Heat shock proteins are generally associated with cellular stress responses and their role is to protect cells from the effects of damaged and misfolded proteins [60–64]. If such proteins persist in the cytoplasm, three chaperone-mediated quality control pathways can be induced: partly denatured proteins can be recognized by heat shock proteins and refolded to retain their function, whereas damaged proteins can be cleared by HSP70-dependent degradation via the proteasome or by chaperone-mediated autophagy [65, 66]. NtFT4 appears to integrate with this system by stabilizing HSP26 levels, which in turn promotes general protein refolding. Moreover, the proteases deregulated by NtFT4 expression in flies may contribute to protein degradation during autophagy. Interestingly, phosphatidylethanolamine (one of the phospholipid ligands of PEBPs) has been shown to induce autophagy, extend the lifespan of *Saccharomyces cerevisiae* [67], and also act as a chaperone for membrane proteins [68, 69].

The small heat shock proteins of Drosophila show functional diversity, with some facilitating protein refolding and others preventing the accumulation of toxic proteins. Regardless of their task in the proteome maintenance system, the overexpression of these diverse small heat shock proteins increased the longevity of fruit flies [34, 70, 71]. Interestingly, NtFT4 not only interacts physically with HSP26 but also upregulates *Hsp26* gene expression. The conspicuous nuclear localization of NtFT4 supports the hypothesis that NtFT4 not only interacts with the cytoplasmic proteostasis machinery but also participates in the transcriptional regulation of its components, which are needed to maintain cell integrity (Supplementary Figure 12). Many proteins found in nuclear speckles, where NtFT4 was enriched, are involved in the regulation of transcription and RNA splicing [72, 73].

In summary, we identified a novel mechanism that connects PEPBs to aging. We found that a plant PEBP (NtFT4) increases longevity in Drosophila by interacting with a number of proteins involved in proteostasis, including HSP26. The functional specificity of different members of the PEBP family highlights their complex molecular interactions, but also provides many opportunities to modulate their activity. NtFT4 also provides a powerful tool to investigate the regulation of proteostasis in animals.

## MATERIALS AND METHODS

### Reagents, plasmids and cloning

All primers used for cloning are listed in Supplementary Table 7. Accession numbers for genes and proteins are listed in Supplementary Table 8. Cloning steps are described in more detail in the Supplementary Methods.

For Drosophila transformation, the NtFT2, NtFT4 and CG7054 coding sequences were amplified by PCR using primers with attached restriction sites, and were transferred to pENTR4 vectors by restriction and ligation. Subsequent transfer to vector pUASTattB_rfA or pUASTattB_rfA_3xHA [28] was achieved by Gateway recombination. Cloning steps for plasmids used in the transfection of yeast, *N. benthamiana* epidermal cells, HEK-293T and S2 cells are provided in the Supplementary Methods.

**Plant cultivation and transformation**

Tobacco (*Nicotiana tabacum* cv. SR1) and Arabidopsis (*Arabidopsis thaliana* ecotype Col-0) plants were cultivated and transformed using the leaf disc method (tobacco) or by floral dip (Arabidopsis) as previously described [18]. Cultivation and transformation details are provided in the Supplementary Methods.

**Bimolecular fluorescence complementation**

Transient expression of split-mRFP and Venus fusion constructs in *N. benthamiana* plants was carried out as previously described [18]. More details are provided in the Supplementary Methods. Fluorescence was analyzed using a TCS SP5 X confocal laser scanning microscope (Leica Microsystems) at excitation/emission wavelengths of 514/525–600 nm for Venus and 543/569–629 nm for reconstituted mRFP. All combinations of split mRFP constructs (C-terminal or N-terminal fusion to CmRFP and NmRFP) were tested. Interaction was confirmed if at least five independent images showing fluorescence were captured.

**Drosophila work**

Flies were raised at 25°C and transgenes were introduced by φC31-based transformation at the landing site *86Fb* [28]. Gain-of-function studies were carried out using the Gal4/UAS system [74]. The driver *da-Gal4* was obtained from the Bloomington stock center. *CG7054* was knocked down using the dsRNA-GD12116 strain obtained from the Vienna stock center (VDRC #40415).

**RING assay**

Negative geotaxis was monitored as previously described [30]. At least 100 male and female flies (10, 30 or 45 days old) were collected in groups of 10 in fresh vials with standard food. After a recovery period of 24 h, they were transferred to test tubes without anesthesia. After 5–10 min to acclimate to the new environment, the tubes were tapped five times in a custom-made device to ensure consistent forces [30]. After impact, the position of each fly within the tube was recorded for 10 s at 10 frames/s. After a 2-min rest period, the tapping process was repeated and the same flies were observed again, for a total of five tests. Images were processed using Fiji with the MTrack3_.jar plugin and AutoRun2.ijm macro. The mean velocity was determined using RING assay Script.R in the R program.

**Immunofluorescence staining of larval tissue**

Tissues were fixed and prepared for immunofluorescence as previously described [75]. The HA-tagged NtFT4 and NtFT2 proteins were detected using a mouse anti-HA antibody (Covance) and anti-mouse IgG coupled to Alexa 488, 568 or 647 (Thermo Fisher Scientific). Nuclei were counterstained with 4′,6-diamidino-2-phenylindole (DAPI). Specimens were analyzed using a Zeiss LSM710 or LSM880 confocal microscope. Original confocal data were processed using ZEN 2012 software (Zeiss), Adobe Photoshop CS6, and Fiji [76].

**Cell culture and transfection**

S2R+ cells (Drosophila Genomics Resource Center, NIH Grant 2P40OD010949) are described herein as S2 cells. The cells were cultivated at 27°C in Schneider's Drosophila medium with 5% fetal calf serum and a 1% antibiotic-antimycotic mix (all from Thermo Fisher Scientific) in six-well plates for transfection and in T25 flasks for subculturing. HEK-293T cells were grown in RPMI-1640 GlutaMAX medium with 5% fetal calf serum and a 1% antibiotic-antimycotic mix in a 5% $CO_2$ atmosphere at 37°C with a relative humidity of ~93%. Cells were transferred to six-well plates in Opti-MEM for transfections using Lipofectamine 3000 (Thermo Fisher Scientific) according to the manufacturer's protocol. To induce expression of constructs using the pMT plasmids, S2 cells were treated with 5 mM $CuSO_4$.

**Protein extraction, analysis and Western blotting**

Proteins for direct immunodetection were extracted from snap-frozen flies, S2 or HEK293T cells using a Tris lysis buffer (Tris-HCl pH 7.5, 150 mM NaCl, 1 mM EDTA, 1% (v/v) NP-40 containing protease and phosphatase inhibitor cocktails). Proteins were separated by SDS-PAGE and transferred to a 0.2-µm nitrocellulose membrane using the wet Mini Trans-Blot Cell system (Bio-Rad Laboratories). Western blots were probed with the following antibodies: anti-HA tag rabbit polyclonal (MBL; #561), anti-Myc tag mouse monoclonal (MBL; #047-3), and anti-HSP26 rabbit polyclonal (custom made, Proteogenix). The primary antibodies were detected using either anti-rabbit/anti-mouse IgG secondary antibodies coupled to alkaline phosphatase (Thermo Fisher Scientific) and SigmaFast BCIP/NBT tablets (Sigma-Aldrich), or anti-rabbit/anti-mouse IgG secondary antibodies coupled to horseradish peroxidase (Thermo Fisher Scientific) and the

SuperSignal West dura kit (Thermo Fisher Scientific). More details are provided in the Supplementary Methods.

**Protein carbonylation analysis**

Whole protein extracts were prepared from adult flies (10 or 30 days old). The total soluble protein concentration was measured using the RotiQuant Universal Kit (Roth), and 2–10 mg of protein was immediately used to measure carbonylation using the Protein Carbonyl Content Assay Kit (Sigma-Aldrich). Protein carbonylation was quantified by normalizing the value against the total protein concentration.

**LC-MS analysis**

For immunoprecipitation, HA-tagged proteins were extracted from the cytosolic and nuclear fractions of transfected S2 cells using hypotonic and hypertonic extraction buffers. Both fractions were combined for subsequent immunoprecipitation using the Pierce Magnetic HA-Tag IP/Co-IP Kit (Thermo Fisher Scientific) according to the manufacturer's acidic elution protocol. Eluates were analyzed by SDS-PAGE and silver staining using Pierce Silver Stain for Mass Spectrometry (Thermo Fisher Scientific) and interacting proteins were identified by LC-MS/MS from the whole eluates and from excised gel bands. Briefly, proteins from the eluates and from gel bands were digested with trypsin [77, 78], acidified with 1% (v/v) trifluoroacetic acid (TFA), desalted [79] and dried in a vacuum centrifuge for storage at –80°C. LC-MS/MS analysis was carried out with reconstituted peptides (2% (v/v) acetonitrile/0.05% (v/v) TFA) using an Ultimate 3000 nanoLC (Thermo Fisher Scientific) coupled via a nanospray interface to a Q Exactive Plus mass spectrometer (Thermo Fisher Scientific). Sample preparation and LC-MS/MS details are provided in the Supplementary Methods.

**Quantitative PCR**

RNA was extracted from flies using the Quick-RNA Tissue/Insect Microprep kit (Zymo Research) and from cells using the NucleoSpin RNA kit (Macherey-Nagel) according to the manufacturers' specifications. Following reverse transcription using PrimeScript RT master mix (Takara Bio), gene expression was analyzed by quantitative real-time PCR using Kapa SYBR Fast qPCR Master Mix and the CFX96 Real-Time System (Bio-Rad Laboratories). Each reaction was carried out in technical triplicates and the primer sequences are provided in Supplementary Table 7. Specificity was ensured by melt curve analysis and the sequencing of PCR products, and by including no-template and no-reverse-transcription controls. Individual PCR efficiency was determined using LinReg PCR v2017.0 [80] and relative gene expression levels were normalized to *Gapdh2* (S2 cells) or to the mean of *Gapdh2*, *14-3-3ε* and *RpL32* (flies).

**Live-cell imaging for subcellular localization**

Localization studies using the pcDNA3 vectors containing constructs HA-EGFP-NtFT4, HA-EGFP-CG7054, HA-EGFP-PEBP1, HA-EGFP-10298, HA-EGFP-CG6180, HA-EGFP-CG17917, HA-EGFP-CG17979 and Myc-mRFP-H2AZ were carried out by co-transfecting HEK-293T cells with EGFP plasmids and pcDNA3-Myc-mRFP-H2AZ using Lipofectamine 3000. Cells in six-well plates were transiently transfected in Opti-MEM medium and fluorescence was imaged in living cells 24 h post-transfection using a TCS SP5 X confocal scanning laser microscope.

**GeneChip analysis**

RNA was extracted from female flies (*da > NtFT4* and *da-Gal4* as a control) at ages of 0–24 h (described herein as 1 day), 5–6 days (5 days) or 10–11 days (10 days) using the Quick-RNA Tissue/Insect Microprep kit, and equimolar amounts representing each age were pooled. Affymetrix GeneChip Drosophila Genome 2.0 Array analysis was carried out by IMGM Laboratories. More details are provided in the Supplementary Methods. For the identification of genes with significant differences in expression in pairwise comparisons, different filtering approaches were tested using both the FDR-corrected *p*-value (Benjamini-Hochberg) and the non-corrected *p*-value from the paired *t*-test. Sequences for subsequent verification of differential gene expression were retrieved from Flybase FB2021_02 [31].

**Yeast-two hybrid screening and drop test**

The initial Y2H screen was carried out using the Matchmaker GoldYeast Two-Hybrid System (Takara Bio), the Mate and Plate Library - *Universal Drosophila (Normalized)* (Takara Bio) and pGBKT7-NtFT2 as a bait construct introduced into *S. cerevisiae* strain Y2HGold using the Yeastmaker transformation system 2 (Takara Bio). To confirm interactions, full-length coding sequences were introduced into pGADT7 and introduced into *S. cerevisiae* Y2HGold cells along with pGBKT7 and applied to drop tests. Co-transformation of pGBKT7-53 and pGADT7-T served as a positive control, and co-transformation of pGBKT7-Lam and pGADT7-T served as a negative control (Takara Bio). Further details are provided in the Supplementary Methods.

### FRET analysis

The *NtFT4* and *CG7054* coding sequences were cloned in-frame with mCerulean (Cer), whereas *CCT7, CG4364, Df31, Hsp26, p47, Pen, Pyk* and *Tsn* were cloned in-frame with mEYFP (EYFP) in vector pcDNA3, with the fluorescent proteins separated from their fusion partners by the linker sequence $(GGGGS)_3$. A fusion of Cer and EYFP in pcDNA3 was prepared as a positive control, whereas Cer or EYFP (each fused only to the linker sequence) were prepared as negative controls. HEK-293T cells were transfected with appropriate combinations of plasmids using Lipofectamine 3000, and FRET was analyzed 24 h post-transfection by flow cytometry using a BD FACSCelesta with BVYG laser configuration (BD Biosciences). The gating strategy and controls are provided in the Supplementary Methods.

### Identification of interaction networks

To integrate NtFT4 into functional networks, its interaction partners were analyzed using Flybase FB2021_02 [31] to identify functional overlaps and they were used for single protein analysis in the String database (https://string-db.org) [32]. Here, interaction sources were set to include interactions based on text mining, experimental evidence, databases, co-expression, neighborhood, gene fusion or co-occurrence.

### Statistical analysis

All boxplots in the figures were prepared in OriginPro2020 v9.7.5.184 (OriginLab) using the default settings (center line = median; box limits = upper and lower quartiles; whiskers = 1.5× interquartile range; points = outliers). Statistical analysis, if not stated otherwise, was carried out using OriginPro2020. Differences in lifespan were analyzed using Kaplan-Meier survival curves and the Mantel-Cox (log-rank) test. Equality of variances was determined by one-way analysis of variance (ANOVA), and pairwise comparisons were assessed using Tukey's *post hoc* test for multiple comparisons and Student's *t*-test for single pairwise comparisons. All *p*-values that could not be provided in figure legends due to space constraints are summarized in Supplementary Table 9.

### Data availability

All data are available upon request. GeneChip data have been deposited in the ArrayExpress database at EMBL-EBI [81] (https://www.ebi.ac.uk/arrayexpress/experiments/E-MTAB-10730/).

## AUTHOR CONTRIBUTIONS

PK, GN, DP and CK conceived and designed the experiments. PK, KS, EN, JK and FB conducted the experiments. PK and CK analyzed the data. DP, PK, GN and CK contributed the reagents, materials, and analytical tools. PK and RT wrote the manuscript. All authors helped to revise the manuscript and approved the submitted version.

## ACKNOWLEDGMENTS

We thank Jost Muth, Christiane Fischer and Andreas Wagner from Fraunhofer IME Aachen for plant cultivation and phenotypic analysis of our tobacco lines. Proteomic data were acquired and analyzed by Susan Hawat and Martin Scholz from the MSPUB of the WWU Münster, which is in part supported by the DFG.

## CONFLICTS OF INTEREST

The authors declare no conflicts of interest related to this study.

## FUNDING

This work was supported by the Fraunhofer Internal Programs under grant no. Attract 125–600318.

## REFERENCES

1. Zeng L, Imamoto A, Rosner MR. Raf kinase inhibitory protein (RKIP): a physiological regulator and future therapeutic target. Expert Opin Ther Targets. 2008; 12:1275–87. https://doi.org/10.1517/14728222.12.10.1275 PMID:18781826

2. Garcia R, Grindlay J, Rath O, Fee F, Kolch W. Regulation of human myoblast differentiation by PEBP4. EMBO Rep. 2009; 10:278–84. https://doi.org/10.1038/embor.2009.4 PMID:19197339

3. Jian W, Bai Y, Li X, Kang J, Lei Y, Xue Y. Phosphatidylethanolamine-binding protein 4 promotes the epithelial-to-mesenchymal transition in non-small cell lung cancer cells by activating the sonic hedgehog signaling pathway. J Cell Biochem. 2019; 120:5386–95. https://doi.org/10.1002/jcb.27817 PMID:30367510

4. Granovsky AE, Rosner MR. Raf kinase inhibitory protein: a signal transduction modulator and

metastasis suppressor. Cell Res. 2008; 18:452–7.
https://doi.org/10.1038/cr.2008.43
PMID:18379591

5. Chatterjee D, Bai Y, Wang Z, Beach S, Mott S, Roy R, Braastad C, Sun Y, Mukhopadhyay A, Aggarwal BB, Darnowski J, Pantazis P, Wyche J, et al. RKIP sensitizes prostate and breast cancer cells to drug-induced apoptosis. J Biol Chem. 2004; 279:17515–23.
https://doi.org/10.1074/jbc.M313816200
PMID:14766752

6. Huang RQ, Wang SQ, Zhu QB, Guo SC, Shi DL, Chen F, Fang YC, Chen R, Lu YC. Knockdown of PEBP4 inhibits human glioma cell growth and invasive potential via ERK1/2 signaling pathway. Mol Carcinog. 2019; 58:135–43.
https://doi.org/10.1002/mc.22915
PMID:30255656

7. George AJ, Holsinger RM, McLean CA, Tan SS, Scott HS, Cardamone T, Cappai R, Masters CL, Li QX. Decreased phosphatidylethanolamine binding protein expression correlates with Abeta accumulation in the Tg2576 mouse model of Alzheimer's disease. Neurobiol Aging. 2006; 27:614–23.
https://doi.org/10.1016/j.neurobiolaging.2005.03.014
PMID:15941609

8. Li H, Huang F, Fan L, Jiang Y, Wang X, Li J, Wang Q, Pan H, Sun J, Cao X, Wang X. Phosphatidylethanolamine-binding protein 4 is associated with breast cancer metastasis through Src-mediated Akt tyrosine phosphorylation. Oncogene. 2014; 33:4589–98.
https://doi.org/10.1038/onc.2013.408
PMID:24276246

9. Taylor S, Pieri K, Nanni P, Tica J, Barratt J, Didangelos A. Phosphatidylethanolamine binding protein-4 (PEBP4) is increased in IgA nephropathy and is associated with IgA-positive B-cells in affected kidneys. J Autoimmun. 2019; 105:102309.
https://doi.org/10.1016/j.jaut.2019.102309
PMID:31402200

10. Bernier I, Tresca JP, Jollès P. Ligand-binding studies with a 23 kDa protein purified from bovine brain cytosol. Biochim Biophys Acta. 1986; 871:19–23.
https://doi.org/10.1016/0167-4838(86)90128-7
PMID:2938633

11. Graveley BR, Brooks AN, Carlson JW, Duff MO, Landolin JM, Yang L, Artieri CG, van Baren MJ, Boley N, Booth BW, Brown JB, Cherbas L, Davis CA, et al. The developmental transcriptome of Drosophila melanogaster. Nature. 2011; 471:473–9.
https://doi.org/10.1038/nature09715
PMID:21179090

12. Pyo JH, Jeon HJ, Park JS, Lee JS, Chung HY, Yoo MA. *Drosophila* PEBP1 inhibits intestinal stem cell aging via suppression of ERK pathway. Oncotarget. 2018; 9:17980–93.
https://doi.org/10.18632/oncotarget.24834
PMID:29719584

13. Vierstraete E, Verleyen P, Baggerman G, D'Hertog W, Van den Bergh G, Arckens L, De Loof A, Schoofs L. A proteomic approach for the analysis of instantly released wound and immune proteins in Drosophila melanogaster hemolymph. Proc Natl Acad Sci U S A. 2004; 101:470–5.
https://doi.org/10.1073/pnas.0304567101
PMID:14707262

14. Levy F, Rabel D, Charlet M, Bulet P, Hoffmann JA, Ehret-Sabatier L. Peptidomic and proteomic analyses of the systemic immune response of Drosophila. Biochimie. 2004; 86:607–16.
https://doi.org/10.1016/j.biochi.2004.07.007
PMID:15556270

15. Rautureau G, Jouvensal L, Decoville M, Locker D, Vovelle F, Schoentgen F. Cloning, high yield over-expression, purification, and characterization of CG18594, a new PEBP/RKIP family member from Drosophila melanogaster. Protein Expr Purif. 2006; 48:90–7.
https://doi.org/10.1016/j.pep.2006.01.020
PMID:16529946

16. Reumer A, Bogaerts A, Van Loy T, Husson SJ, Temmerman L, Choi C, Clynen E, Hassan B, Schoofs L. Unraveling the protective effect of a Drosophila phosphatidylethanolamine-binding protein upon bacterial infection by means of proteomics. Dev Comp Immunol. 2009; 33:1186–95.
https://doi.org/10.1016/j.dci.2009.06.010
PMID:19545586

17. Karlgren A, Gyllenstrand N, Källman T, Sundström JF, Moore D, Lascoux M, Lagercrantz U. Evolution of the PEBP gene family in plants: functional diversification in seed plant evolution. Plant Physiol. 2011; 156:1967–77.
https://doi.org/10.1104/pp.111.176206
PMID:21642442

18. Harig L, Beinecke FA, Oltmanns J, Muth J, Müller O, Rüping B, Twyman RM, Fischer R, Prüfer D, Noll GA. Proteins from the FLOWERING LOCUS T-like subclade of the PEBP family act antagonistically to regulate floral initiation in tobacco. Plant J. 2012; 72:908–21.
https://doi.org/10.1111/j.1365-313X.2012.05125.x
PMID:22889438

19. Schmidt FJ, Zimmermann MM, Wiedmann DR, Lichtenauer S, Grundmann L, Muth J, Twyman RM,

` Prüfer D, Noll GA. The Major Floral Promoter NtFT5 in Tobacco (*Nicotiana tabacum*) Is a Promising Target for Crop Improvement. Front Plant Sci. 2020; 10:1666.
https://doi.org/10.3389/fpls.2019.01666
PMID:31998348

20. Lifschitz E, Ayre BG, Eshed Y. Florigen and anti-florigen - a systemic mechanism for coordinating growth and termination in flowering plants. Front Plant Sci. 2014; 5:465.
https://doi.org/10.3389/fpls.2014.00465
PMID:25278944

21. Pin PA, Benlloch R, Bonnet D, Wremerth-Weich E, Kraft T, Gielen JJ, Nilsson O. An antagonistic pair of FT homologs mediates the control of flowering time in sugar beet. Science. 2010; 330:1397–400.
https://doi.org/10.1126/science.1197004
PMID:21127254

22. Pnueli L, Gutfinger T, Hareven D, Ben-Naim O, Ron N, Adir N, Lifschitz E. Tomato SP-interacting proteins define a conserved signaling system that regulates shoot architecture and flowering. Plant Cell. 2001; 13:2687–702.
https://doi.org/10.1105/tpc.010293
PMID:11752381

23. Silva WB, Vicente MH, Robledo JM, Reartes DS, Ferrari RC, Bianchetti R, Araújo WL, Freschi L, Peres LEP, Zsögön A. SELF-PRUNING Acts Synergistically with DIAGEOTROPICA to Guide Auxin Responses and Proper Growth Form. Plant Physiol. 2018; 176:2904–16.
https://doi.org/10.1104/pp.18.00038
PMID:29500181

24. Ho WW, Weigel D. Structural features determining flower-promoting activity of Arabidopsis FLOWERING LOCUS T. Plant Cell. 2014; 26:552–64.
https://doi.org/10.1105/tpc.113.115220
PMID:24532592

25. Banfield MJ, Brady RL. The structure of Antirrhinum centroradialis protein (CEN) suggests a role as a kinase regulator. J Mol Biol. 2000; 297:1159–70.
https://doi.org/10.1006/jmbi.2000.3619
PMID:10764580

26. Ahn JH, Miller D, Winter VJ, Banfield MJ, Lee JH, Yoo SY, Henz SR, Brady RL, Weigel D. A divergent external loop confers antagonistic activity on floral regulators FT and TFL1. EMBO J. 2006; 25:605–14.
https://doi.org/10.1038/sj.emboj.7600950
PMID:16424903

27. Wang Z, Yang R, Devisetty UK, Maloof JN, Zuo Y, Li J, Shen Y, Zhao J, Bao M, Ning G. The Divergence of Flowering Time Modulated by *FT/TFL1* Is Independent to Their Interaction and Binding Activities. Front Plant Sci. 2017; 8:697.
https://doi.org/10.3389/fpls.2017.00697
PMID:28533784

28. Bischof J, Maeda RK, Hediger M, Karch F, Basler K. An optimized transgenesis system for Drosophila using germ-line-specific phiC31 integrases. Proc Natl Acad Sci U S A. 2007; 104:3312–7.
https://doi.org/10.1073/pnas.0611511104
PMID:17360644

29. Schnorrer F, Schönbauer C, Langer CC, Dietzl G, Novatchkova M, Schernhuber K, Fellner M, Azaryan A, Radolf M, Stark A, Keleman K, Dickson BJ. Systematic genetic analysis of muscle morphogenesis and function in Drosophila. Nature. 2010; 464:287–91.
https://doi.org/10.1038/nature08799
PMID:20220848

30. Gargano JW, Martin I, Bhandari P, Grotewiel MS. Rapid iterative negative geotaxis (RING): a new method for assessing age-related locomotor decline in Drosophila. Exp Gerontol. 2005; 40:386–95.
https://doi.org/10.1016/j.exger.2005.02.005
PMID:15919590

31. Larkin A, Marygold SJ, Antonazzo G, Attrill H, Dos Santos G, Garapati PV, Goodman JL, Gramates LS, Millburn G, Strelets VB, Tabone CJ, Thurmond J, and FlyBase Consortium. FlyBase: updates to the Drosophila melanogaster knowledge base. Nucleic Acids Res. 2021; 49:D899–907.
https://doi.org/10.1093/nar/gkaa1026
PMID:33219682

32. Szklarczyk D, Gable AL, Lyon D, Junge A, Wyder S, Huerta-Cepas J, Simonovic M, Doncheva NT, Morris JH, Bork P, Jensen LJ, Mering CV. STRING v11: protein-protein association networks with increased coverage, supporting functional discovery in genome-wide experimental datasets. Nucleic Acids Res. 2019; 47:D607–13.
https://doi.org/10.1093/nar/gky1131
PMID:30476243

33. Cho SC, Park MC, Keam B, Choi JM, Cho Y, Hyun S, Park SC, Lee J. DDS, 4,4'-diaminodiphenylsulfone, extends organismic lifespan. Proc Natl Acad Sci U S A. 2010; 107:19326–31.
https://doi.org/10.1073/pnas.1005078107
PMID:20974969

34. Wang HD, Kazemi-Esfarjani P, Benzer S. Multiple-stress analysis for isolation of Drosophila longevity genes. Proc Natl Acad Sci U S A. 2004; 101:12610–5.
https://doi.org/10.1073/pnas.0404648101
PMID:15308776

35. Zou S, Meadows S, Sharp L, Jan LY, Jan YN. Genome-wide study of aging and oxidative stress response in Drosophila melanogaster. Proc Natl Acad Sci U S A. 2000; 97:13726–31.
https://doi.org/10.1073/pnas.260496697
PMID:11095759

36. Cao X, Jiang H. Building a platform for predicting functions of serine protease-related proteins in Drosophila melanogaster and other insects. Insect Biochem Mol Biol. 2018; 103:53–69.
https://doi.org/10.1016/j.ibmb.2018.10.006
PMID:30367934

37. Garrett M, Fullaondo A, Troxler L, Micklem G, Gubb D. Identification and analysis of serpin-family genes by homology and synteny across the 12 sequenced Drosophilid genomes. BMC Genomics. 2009; 10:489.
https://doi.org/10.1186/1471-2164-10-489
PMID:19849829

38. Rautureau GJ, Vovelle F, Schoentgen F, Decoville M, Locker D, Damblon C, Jouvensal L. NMR structure of a phosphatidyl-ethanolamine binding protein from Drosophila. Proteins. 2010; 78:1606–10.
https://doi.org/10.1002/prot.22682
PMID:20131378

39. Kim SJ, Hong SM, Yoo SJ, Moon S, Jung HS, Ahn JH. Post-Translational Regulation of FLOWERING LOCUS T Protein in Arabidopsis. Mol Plant. 2016; 9:308–11.
https://doi.org/10.1016/j.molp.2015.11.001
PMID:26548373

40. Kronenberg J, Schrödter K, Noll GA, Twyman RM, Prüfer D, Känel P. The tobacco phosphatidylethanolamine-binding protein NtFT4 simultaneously improves vitality, growth, and protein yield in human cells. Biotechnol Bioeng. 2021; 118:3770–86.
https://doi.org/10.1002/bit.27853
PMID:34110007

41. Hipp MS, Kasturi P, Hartl FU. The proteostasis network and its decline in ageing. Nat Rev Mol Cell Biol. 2019; 20:421–35.
https://doi.org/10.1038/s41580-019-0101-y
PMID:30733602

42. He H, Liu D, Lin H, Jiang S, Ying Y, Chun S, Deng H, Zaia J, Wen R, Luo Z. Phosphatidylethanolamine binding protein 4 (PEBP4) is a secreted protein and has multiple functions. Biochim Biophys Acta. 2016; 1863:1682–9.
https://doi.org/10.1016/j.bbamcr.2016.03.022
PMID:27033522

43. Granovsky AE, Clark MC, McElheny D, Heil G, Hong J, Liu X, Kim Y, Joachimiak G, Joachimiak A, Koide S, Rosner MR. Raf kinase inhibitory protein function is regulated via a flexible pocket and novel phosphorylation-dependent mechanism. Mol Cell Biol. 2009; 29:1306–20.
https://doi.org/10.1128/MCB.01271-08
PMID:19103740

44. Rath O, Park S, Tang HH, Banfield MJ, Brady RL, Lee YC, Dignam JD, Sedivy JM, Kolch W, Yeung KC. The RKIP (Raf-1 Kinase Inhibitor Protein) conserved pocket binds to the phosphorylated N-region of Raf-1 and inhibits the Raf-1-mediated activated phosphorylation of MEK. Cell Signal. 2008; 20:935–41.
https://doi.org/10.1016/j.cellsig.2008.01.012
PMID:18294816

45. Al-Mulla F, Bitar MS, Taqi Z, Yeung KC. RKIP: much more than Raf kinase inhibitory protein. J Cell Physiol. 2013; 228:1688–702.
https://doi.org/10.1002/jcp.24335
PMID:23359513

46. Mummery-Widmer JL, Yamazaki M, Stoeger T, Novatchkova M, Bhalerao S, Chen D, Dietzl G, Dickson BJ, Knoblich JA. Genome-wide analysis of Notch signalling in Drosophila by transgenic RNAi. Nature. 2009; 458:987–92.
https://doi.org/10.1038/nature07936
PMID:19363474

47. Dietzl G, Chen D, Schnorrer F, Su KC, Barinova Y, Fellner M, Gasser B, Kinsey K, Oppel S, Scheiblauer S, Couto A, Marra V, Keleman K, Dickson BJ. A genome-wide transgenic RNAi library for conditional gene inactivation in Drosophila. Nature. 2007; 448:151–6.
https://doi.org/10.1038/nature05954
PMID:17625558

48. Jones MA, Grotewiel M. Drosophila as a model for age-related impairment in locomotor and other behaviors. Exp Gerontol. 2011; 46:320–5.
https://doi.org/10.1016/j.exger.2010.08.012
PMID:20800672

49. Glatter T, Schittenhelm RB, Rinner O, Roguska K, Wepf A, Jünger MA, Köhler K, Jevtov I, Choi H, Schmidt A, Nesvizhskii AI, Stocker H, Hafen E, et al. Modularity and hormone sensitivity of the Drosophila melanogaster insulin receptor/target of rapamycin interaction proteome. Mol Syst Biol. 2011; 7:547.
https://doi.org/10.1038/msb.2011.79
PMID:22068330

50. Saucedo LJ, Gao X, Chiarelli DA, Li L, Pan D, Edgar BA. Rheb promotes cell growth as a component of the insulin/TOR signalling network. Nat Cell Biol. 2003; 5:566–71.
https://doi.org/10.1038/ncb996
PMID:12766776

51. Stocker H, Radimerski T, Schindelholz B, Wittwer F, Belawat P, Daram P, Breuer S, Thomas G, Hafen E. Rheb is an essential regulator of S6K in controlling cell growth in Drosophila. Nat Cell Biol. 2003; 5:559–65. https://doi.org/10.1038/ncb995 PMID:12766775

52. Le TP, Vuong LT, Kim AR, Hsu YC, Choi KW. 14-3-3 proteins regulate Tctp-Rheb interaction for organ growth in Drosophila. Nat Commun. 2016; 7:11501. https://doi.org/10.1038/ncomms11501 PMID:27151460

53. Dibble CC, Cantley LC. Regulation of mTORC1 by PI3K signaling. Trends Cell Biol. 2015; 25:545–55. https://doi.org/10.1016/j.tcb.2015.06.002 PMID:26159692

54. Long X, Lin Y, Ortiz-Vega S, Yonezawa K, Avruch J. Rheb binds and regulates the mTOR kinase. Curr Biol. 2005; 15:702–13. https://doi.org/10.1016/j.cub.2005.02.053 PMID:15854902

55. Vinayagam A, Kulkarni MM, Sopko R, Sun X, Hu Y, Nand A, Villalta C, Moghimi A, Yang X, Mohr SE, Hong P, Asara JM, Perrimon N. An Integrative Analysis of the InR/PI3K/Akt Network Identifies the Dynamic Response to Insulin Signaling. Cell Rep. 2016; 16:3062–74. https://doi.org/10.1016/j.celrep.2016.08.029 PMID:27626673

56. Kapahi P, Zid BM, Harper T, Koslover D, Sapin V, Benzer S. Regulation of lifespan in Drosophila by modulation of genes in the TOR signaling pathway. Curr Biol. 2004; 14:885–90. https://doi.org/10.1016/j.cub.2004.03.059 PMID:15186745

57. Partridge L, Alic N, Bjedov I, Piper MD. Ageing in Drosophila: the role of the insulin/Igf and TOR signalling network. Exp Gerontol. 2011; 46:376–81. https://doi.org/10.1016/j.exger.2010.09.003 PMID:20849947

58. Antikainen H, Driscoll M, Haspel G, Dobrowolski R. TOR-mediated regulation of metabolism in aging. Aging Cell. 2017; 16:1219–33. https://doi.org/10.1111/acel.12689 PMID:28971552

59. Abe Y, Yoon SO, Kubota K, Mendoza MC, Gygi SP, Blenis J. p90 ribosomal S6 kinase and p70 ribosomal S6 kinase link phosphorylation of the eukaryotic chaperonin containing TCP-1 to growth factor, insulin, and nutrient signaling. J Biol Chem. 2009; 284:14939–48. https://doi.org/10.1074/jbc.M900097200 PMID:19332537

60. Koteiche HA, McHaourab HS. Mechanism of chaperone function in small heat-shock proteins. Phosphorylation-induced activation of two-mode binding in alphaB-crystallin. J Biol Chem. 2003; 278:10361–7. https://doi.org/10.1074/jbc.M211851200 PMID:12529319

61. Haslbeck M, Franzmann T, Weinfurtner D, Buchner J. Some like it hot: the structure and function of small heat-shock proteins. Nat Struct Mol Biol. 2005; 12:842–6. https://doi.org/10.1038/nsmb993 PMID:16205709

62. Basha E, O'Neill H, Vierling E. Small heat shock proteins and α-crystallins: dynamic proteins with flexible functions. Trends Biochem Sci. 2012; 37:106–17. https://doi.org/10.1016/j.tibs.2011.11.005 PMID:22177323

63. Haslbeck M, Vierling E. A first line of stress defense: small heat shock proteins and their function in protein homeostasis. J Mol Biol. 2015; 427:1537–48. https://doi.org/10.1016/j.jmb.2015.02.002 PMID:25681016

64. Bakthisaran R, Akula KK, Tangirala R, Rao CM. Phosphorylation of αB-crystallin: Role in stress, aging and patho-physiological conditions. Biochim Biophys Acta. 2016; 1860:167–82. https://doi.org/10.1016/j.bbagen.2015.09.017 PMID:26415747

65. Calderwood SK, Murshid A, Prince T. The shock of aging: molecular chaperones and the heat shock response in longevity and aging--a mini-review. Gerontology. 2009; 55:550–8. https://doi.org/10.1159/000225957 PMID:19546513

66. Lei Y, Liu K, Hou L, Ding L, Li Y, Liu L. Small chaperons and autophagy protected neurons from necrotic cell death. Sci Rep. 2017; 7:5650. https://doi.org/10.1038/s41598-017-05995-6 PMID:28720827

67. Rockenfeller P, Koska M, Pietrocola F, Minois N, Knittelfelder O, Sica V, Franz J, Carmona-Gutierrez D, Kroemer G, Madeo F. Phosphatidylethanolamine positively regulates autophagy and longevity. Cell Death Differ. 2015; 22:499–508. https://doi.org/10.1038/cdd.2014.219 PMID:25571976

68. Bogdanov M, Dowhan W. Lipid-assisted protein folding. J Biol Chem. 1999; 274:36827–30. https://doi.org/10.1074/jbc.274.52.36827 PMID:10601231

69. Patel D, Witt SN. Ethanolamine and Phosphatidylethanolamine: Partners in Health and Disease. Oxid Med Cell Longev. 2017; 2017:4829180. https://doi.org/10.1155/2017/4829180 PMID:28785375

70. Vos MJ, Carra S, Kanon B, Bosveld F, Klauke K, Sibon OC, Kampinga HH. Specific protein homeostatic functions of small heat-shock proteins increase lifespan. Aging Cell. 2016; 15:217–26. https://doi.org/10.1111/acel.12422 PMID:26705243

71. Morrow G, Heikkila JJ, Tanguay RM. Differences in the chaperone-like activities of the four main small heat shock proteins of Drosophila melanogaster. Cell Stress Chaperones. 2006; 11:51–60. PMID:16572729

72. Galganski L, Urbanek MO, Krzyzosiak WJ. Nuclear speckles: molecular organization, biological function and role in disease. Nucleic Acids Res. 2017; 45:10350–68. https://doi.org/10.1093/nar/gkx759 PMID:28977640

73. Chen Y, Belmont AS. Genome organization around nuclear speckles. Curr Opin Genet Dev. 2019; 55:91–9. https://doi.org/10.1016/j.gde.2019.06.008 PMID:31394307

74. Brand AH, Perrimon N. Targeted gene expression as a means of altering cell fates and generating dominant phenotypes. Development. 1993; 118:401–15. https://doi.org/10.1242/dev.118.2.401 PMID:8223268

75. Yuva-Aydemir Y, Bauke AC, Klämbt C. Spinster controls Dpp signaling during glial migration in the Drosophila eye. J Neurosci. 2011; 31:7005–15. https://doi.org/10.1523/JNEUROSCI.0459-11.2011 PMID:21562262

76. Schindelin J, Arganda-Carreras I, Frise E, Kaynig V, Longair M, Pietzsch T, Preibisch S, Rueden C, Saalfeld S, Schmid B, Tinevez JY, White DJ, Hartenstein V, et al. Fiji: an open-source platform for biological-image analysis. Nat Methods. 2012; 9:676–82. https://doi.org/10.1038/nmeth.2019 PMID:22743772

77. Wiśniewski JR, Zougman A, Nagaraj N, Mann M. Universal sample preparation method for proteome analysis. Nat Methods. 2009; 6:359–62. https://doi.org/10.1038/nmeth.1322 PMID:19377485

78. Shevchenko A, Tomas H, Havlis J, Olsen JV, Mann M. In-gel digestion for mass spectrometric characterization of proteins and proteomes. Nat Protoc. 2006; 1:2856–60. https://doi.org/10.1038/nprot.2006.468 PMID:17406544

79. Rappsilber J, Mann M, Ishihama Y. Protocol for micro-purification, enrichment, pre-fractionation and storage of peptides for proteomics using StageTips. Nat Protoc. 2007; 2:1896–906. https://doi.org/10.1038/nprot.2007.261 PMID:17703201

80. Ruijter JM, Ramakers C, Hoogaars WM, Karlen Y, Bakker O, van den Hoff MJ, Moorman AF. Amplification efficiency: linking baseline and bias in the analysis of quantitative PCR data. Nucleic Acids Res. 2009; 37:e45. https://doi.org/10.1093/nar/gkp045 PMID:19237396

81. Kaenel P, Noll GA, Schroedter K, Naffin E, Kronenberg J, Busswinkel F, Twyman RM, Klämbt C, Prüfer D. GeneChip array of female D. melanogaster expressing tobacco NtFT4. ArrayExpress. 2021; E-MTAB-10730. https://www.ebi.ac.uk/arrayexpress/experiments/E-MTAB-10730

## SUPPLEMENTARY MATERIALS

### Supplementary Methods

**Cloning**

To create stable plant lines expressing different PEBPs, we used the binary plasmids pLab12.1 [1] for Arabidopsis and pBIN19 [2] for tobacco. The coding sequences of human RKIP and PEBP4 (also known as hPEBP4), tobacco NtFT2 and NtFT4, and Drosophila PEBP1 and CG7054 were amplified by PCR using primers with attached restriction sites (corresponding restriction sites are noted in the primer names, and all restriction enzymes were from New England Biolabs), and were transferred to vectors pLab12.1 or pRT104 [3] by restriction and ligation. A variant of CG7054 containing part of NtFT4 (including the YAPGW and EVYN motifs in segment B) was prepared by splice overlap extension PCR and subsequent cloning as described for the other PEBPs (Supplementary Figure 1). The expression cassettes were transferred to pRT104, released with HindIII, and ligated into the final destination vector pBIN19.

For Drosophila transformation, the NtFT2, NtFT4 and CG7054 coding sequences were amplified by PCR using primers with attached restriction sites, and were transferred to pENTR4 vectors (Thermo Fisher Scientific) by restriction and ligation. Subsequent transfer to vector pUASTattB_rfA or pUASTattB_rfA_3xHA [4] was achieved by Gateway recombination.

For Y2H and BiFC assays, the coding sequences of NtFT2, NtFT4, NtFD1, 14-3-3 a-1, 14-3-3 c, 14-3-3 d, 14-3-3 e-2, 14-3-3 f, 14-3-3 f-1, 14-3-3 g and 14-3-3 i-2 from tobacco as well as 4E-T, Act42A, Cals, CCT7, CG3303, CG4364, CG5028, CG6523, CG7054, CG7220, CG11148, CG13775, CG31644, CKIIα-i3, Df31, DhpD, Dpr7, Eip55E, Hsp26, Idgf3, mRpL44, Nplp4, Nrv2, Nrv3, p47, Pen, PyK, Rheb, Rps10b, Tsn, Wech, Yippee and ε-Try from Drosophila were amplified from cDNA using primers with attached restriction sites, and transferred to vectors pGBKT7 or pGADT7 (Takara) or to pENTR4. Subsequent transfer to pBatTL vectors was achieved by Gateway recombination (BatTL plasmids were kindly provided by Joachim Uhrig and Guido Jach, University of Cologne, Cologne, Germany).

For transient expression in HEK-293T or S2 cells, the codon-optimized NtFT4 and NtFT2 coding sequences were synthesized as Gene Strings by Thermo Fisher Scientific, cloned in-frame with HA-EGFP, and transferred to vector pMT-puro (a gift from David Sabatini, Addgene plasmid # 17923; http://n2t.net/addgene:17923; RRID:Addgene_17923) or pcDNA3 (pcDNA3-EGFP was a gift from Doug Golenbock, Addgene plasmid # 13031; http://n2t.net/addgene:13031; RRID:Addgene_13031) by amplifying each segment, digesting the products with restriction enzymes SpeI/XhoI (HA-EGFP), XhoI/ApaI (NtFT4 or NtFT2) and SpeI/ApaI (pMT or pcDNA3 backbone) and ligating them. Accordingly, the Drosophila PEBPs CG7054 and PEBP1 and the putative interaction partners (14-3-3 ζ, Cbs, CCT2, CCT7, CG4364, Df31, HSP26, p47, Pen, PyK, Rack1, Tsn) for co-immunoprecipitation were amplified from cDNA and transferred by restriction and ligation into pMT-puro or pcDNA3. HA without EGFP and Myc tags was added to the coding sequences by PCR.

**Plant cultivation and transformation**

Tobacco (*Nicotiana tabacum* cv. SR1) seeds were sown and the plants were cultivated in soil under long-day conditions in the greenhouse (16-h photoperiod, artificial light switched on if natural light fell below 700 µmol $m^{-2}$ $s^{-1}$, 22–25°C under light, 19–25°C in the dark). Stable transformation was carried out using the leaf disc method [5] with *Agrobacterium tumefaciens* strain LBA4404 [6]. For the selection of transgenic plants, MS medium was supplemented with 100 mg/L kanamycin. After callus regeneration and rooting in sterile culture medium, independent transgenic plant lines were cultivated in the greenhouse as stated above.

Arabidopsis (*Arabidopsis thaliana* ecotype Col-0) plants were cultivated in a York phytochamber at 23°C with a 16-h photoperiod (20 klx light intensity). Transformation was carried out by floral dip using *A. tumefaciens* EHA105 carrying the appropriate binary plasmids [7]. For the selection of transgenic plants, seeds were sown and seedlings were sprayed 2–3 times with glufosinate ammonium (trade name Basta).

**Bimolecular fluorescence complementation**

For the transient expression of split-mRFP and Venus fusion constructs, *A. tumefaciens* strain GV3101 pMP90 was transformed with the corresponding binary pBatTL destination vector by electroporation. *N. benthamiana* plants were cultivated in the greenhouse (16-h photoperiod) until they were 3–4 weeks old before infiltrating the leaves with *A. tumefaciens* strain GV3101 pMP90 carrying the appropriate pBatTL plasmids and *A. tumefaciens* strain C58C1 carrying the pCH32 helper plasmid and the pBin61 plasmid encoding the RNA silencing suppressor p19 from tomato bushy stunt virus [8]. Plants were cultivated under continuous light for 3–4 days, and leaf discs were screened for fluorescent cells in the abaxial epidermis.

**Yeast-two hybrid screening and drop test**

The initial Y2H screen was carried out using the Matchmaker GoldYeast Two-Hybrid System (Takara Bio), the Mate and Plate Library - *Universal Drosophila (Normalized)* (Takara Bio) and pGBKT7-NtFT2 as a bait construct introduced into *S. cerevisiae* strain Y2HGold according to the manufacturer's protocol (Takara Bio). Plasmids were isolated from positive colonies using the Zymoprep Yeast Plasmid Miniprep I kit (Zymo Research) for sequencing. To confirm interactions, full-length coding sequences were introduced into pGADT7 and introduced into *S. cerevisiae* Y2HGold cells along with pGBKT7. Transformed colonies were selected by growth on double dropout (DDO) medium plates (SD –leucine –tryptophan) (Takara Bio). For drop tests, yeast strains were grown in 3 mL DDO liquid medium at 30°C until they reached $OD_{600}$ = 1, then 10 µL of the undiluted culture and 1:10, 1:100 and 1:1000 dilutions) was dropped onto selective quadruple dropout medium (SD –leucine –tryptophan –adenine –histidine) containing 200 ng/mL aureobasidin A (Takara Bio) and incubated at 30°C until colony growth was clearly observed for the positive control.

**GeneChip analysis**

After measuring the RNA concentration and purity on a NanoDrop ND-1000 spectral photometer (Peqlab), RNA integrity was confirmed by capillary electrophoresis using a 2100 Bioanalyzer and the RNA 6000 Nano LabChip Kit (Agilent Technologies). We introduced 200 ng total RNA per sample into an RT-IVT reaction after spiking the RNA samples with polyadenylated transcripts using the Gene Chip Poly-A Control kit (Affymetrix) serving as an internal labeling control for linearity, sensitivity and accuracy.

The spiked total RNA was reverse transcribed into cDNA and then converted into biotin-labeled antisense RNA by 16-h *in vitro* transcription using the 3′IVT Expression kit (Affymetrix). The resulting single-stranded antisense RNA was purified and fragmented. Following the validation of antisense RNA quality, the labeled and fragmented RNA was spiked with cDNA hybridization controls (GeneChip Hybridization Control Kit, Affymetrix). The spiked RNA samples were hybridized at 45°C for 16 h on separate Affymetrix GeneChip Drosophila Genome 2.0 Arrays.

After hybridization, microarrays were stained in two binding cycles using anti-biotin antibodies and streptavidin, R-phycoerythrin conjugate. The microarrays were then washed with increasing stringency and conserved in holding buffer using the Affymetrix GeneChip 3000 Fluidics Station in combination with the Affymetrix GeneChip Command Console (AGCC) – Fluidics Control Software v4.0.0.1567. Fluorescence was detected using the Affymetrix GeneChip 3000 Scanner and AGCC Scan Control Software v4.0.0.1567 (Affymetrix). The software tool GeneSpring GX13.1 (Agilent Technologies) was used for quality control, statistical data analysis, visualization and differential expression analysis. The Robust Multi-Array Analysis (RMA) algorithm was applied for summarization and quantile normalization of the dataset. Pearson's correlation coefficients (r) were calculated for all pairwise comparisons.

**Protein extraction, analysis and Western blotting**

For protein extraction and direct immunodetection, snap-frozen flies were homogenized in ice-cold lysis buffer (Tris-HCl pH 7.5, 150 mM NaCl, 1 mM EDTA, 1% (v/v) NP-40 containing protease and phosphatase inhibitor cocktails) using a micro-pistil, and S2 or HEK-293T cell pellets were lysed without homogenization. For the isolation of total proteins to test protein carbonylation, snap-frozen flies were homogenized in ice-cold lysis buffer 2 (20 mM HEPES pH 7.9, 420 mM NaCl, 1.5 mM $MgCl_2$, 0.2 mM EDTA, 1 mM DTT, 25 % (v/v) glycerol containing protease and phosphatase inhibitor cocktails) using a micro-pistil, followed by two freeze-thaw cycles (–20/95°C) and three rounds of sonication for 30 s in a water bath. After these homogenization procedures, proteins were extracted on ice for 30 min and debris was removed by centrifugation (20,000 × g, 20 min, 4°C). Protein concentrations in the extracts were measured using the Pierce Coomassie Plus Protein Assay (Thermo Fisher Scientific) or the RotiQuant Universal assay (Roth) according to the manufacturers' recommendations. Proteins were separated by SDS-PAGE and stained using the PAGE Blue protein staining kit or transferred to a 0.2-µm nitrocellulose membrane using the wet Mini Trans-Blot Cell system (Bio-Rad Laboratories). Transfer and comparable protein loading were controlled by staining blots with Ponceau S or the Pierce Reversible Protein Stain Kit for Nitrocellulose Membranes (Thermo Fisher Scientific). Anti-HSP26 rabbit polyclonal antibodies were custom made using three peptides (VDELQEPRSPIYEL, LPLGTQQRRSINGC and VLALRREMANRND) for immunization (Proteogenix). All primary antibodies were detected using either anti-rabbit/anti-mouse IgG secondary antibodies coupled to AP (Thermo Fisher Scientific) and SigmaFast BCIP/NBT tablets (Sigma-Aldrich), or anti-rabbit/anti-mouse IgG secondary antibodies coupled to HRP (Thermo Fisher Scientific) and the SuperSignal West dura kit (Thermo Fisher Scientific). The signals from the SuperSignal West dura kit were detected using a G:Box Chemi (Syngene). Brightness and contrast were optimized using Adobe Photoshop CS6 v13.0.1 × 64 (Adobe Systems).

**Protein extraction and LC-MS analysis**

Transiently transfected cells were harvested by aspiration, washed with cold PBS and proteins were extracted in two steps under mild conditions to maintain interaction complexes. First, cells were resuspended in a hypotonic buffer to extract cytoplasmic proteins (10 mM HEPES pH 7.9, 10 mM KCl, 1.5 mM $MgCl_2$, 1 mM DTT containing protease and phosphatase inhibitor cocktails) for 30 min on ice. Cytoplasmic proteins were collected in the supernatant by centrifugation (4000 × g, 10 min, 4°C) and the nuclear pellet fraction was resuspended in extraction buffer (20 mM HEPES pH 7.9, 420 mM NaCl, 25% (v/v) glycerol, 1.5 mM $MgCl_2$, 1 mM DTT, 0.2 mM EDTA containing protease and phosphatase inhibitor cocktails). Nuclear proteins were extracted by shaking for 30 min at 4°C. Cell fragments were removed by centrifugation (20,000 × g, 20 min, 4°C). Both fractions were combined for immunoprecipitation using the Pierce Magnetic HA-Tag IP/Co-IP Kit (Thermo Fisher Scientific) according to the manufacturer's acidic elution protocol. Eluates were analyzed by SDS-PAGE and silver staining using Pierce Silver Stain for Mass Spectrometry (Thermo Fisher Scientific) and interacting proteins were identified by LC-MS/MS.

Protein concentrations in the eluates were determined using the Pierce BCA protein assay kit (Thermo Fisher Scientific) against a bovine serum albumin (BSA) standard curve. We digested 25 µg of protein per bait sample using trypsin according to the FASP protocol [9]. After overnight digestion, samples were acidified with 1% (v/v) trifluoroacetic acid (TFA). A peptide sample aliquot corresponding to 5 µg of digested protein was desalted using self-packed StageTips [10]. Desalted samples were dried in a vacuum centrifuge and stored at –80°C. Excised silver-stained gel bands were destained and digested with trypsin [11], without reduction and alkylation of cysteines. Extracted peptides were acidified, desalted with StageTips and stored as described above. LC-MS/MS analysis was carried out using an Ultimate 3000 nanoLC (Thermo Fisher Scientific) coupled via a nanospray interface to a Q Exactive Plus mass spectrometer (Thermo Fisher Scientific).

Prior to LC-MS/MS analysis, samples were reconstituted in 2% (v/v) acetonitrile/0.05% (v/v) TFA to a (theoretical) concentration of 0.5 µg/µL. Samples (2 µL) were loaded on a trap column (C18, Acclaim PepMap 100, 300 µM × 5 mm, 5 µm particle size, 100 Å pore size; Thermo Fisher Scientific) at a flow rate of 10 µL/min for 3 min using 2% (v/v) acetonitrile/0.05% (v/v) TFA in ultrapure water. The peptides were separated on a reversed-phase column (C18, Acclaim Pepmap C18, 75 µm × 50 cm, 2 µm particle size, 100 Å pore size; Thermo Fisher Scientific) at a flow rate of 250 nL/min. Eluents were composed of 0.1% (v/v) formic acid in ultrapure water (A) and 80% (v/v) acetonitrile/0.1% (v/v) formic acid in ultrapure water (B). The following gradient was applied: 2.5–18% B over 60 min, 18–35% B over 40 min, 35–99% B over 5 min, 99% B for 20 min. The mass spectrometer was operated in positive ion mode. MS full scans (MS1, *m/z* 350–1400) were acquired at a resolution of 70,000 (FWHM, at *m/z* 200) with internal lock mass calibration on *m/z* 445.120025. The AGC target and maximum injection time were set to $3 \times 10^6$ and 50 ms, respectively. For $MS^2$, the 12 most intense ions with charge states 2–4 were fragmented by higher-energy c-trap dissociation (HCD) at 27% normalized collision energy. Dynamic exclusion was set to "auto" (chromatographic peak width 15 s) with a precursor tolerance of 5 ppm. $MS^2$ spectra were recorded at a resolution of 17,500. The AGC target was $5 \times 10^4$, the minimum AGC target was $5 \times 10^2$, the maximum injection time was 50 ms, and the precursor isolation window was 1.5 *m/z*.

After in-gel digestion, dried peptides were dissolved in 6 µL 2% (v/v) acetonitrile/0.05% (v/v) TFA and 2 µL was loaded on a trap column. Samples were analyzed as described above, with the following modifications: the AGC target minimum and maximum injection time for $MS^2$ were set to $5.5 \times 10^2$ and 55 ms, respectively. Ions with charged states 2–5 were fragmented. The gradient for peptide separation was programmed as follows: 2.5–45% B over 40 min, 45–99% B over 5 min, 99% B for 20 min.

Database searching and label-free quantification were carried out in Proteome Discoverer v2.2 (Thermo Fisher Scientific). Spectral files were searched using SequestHT against a *D. melanogaster* protein list (UniProt proteome: AUP000000803, downloaded 2018-06–26), supplemented with a list of common contaminants (cRAP, https://www.thegpm.org/crap/) and the polypeptide sequence of recombinant EGFP-NtFT4. Precursor and fragment mass tolerances were set to 10 ppm and 0.02 Da, respectively. The minimum peptide length was six and a maximum of two missed cleavages was allowed. Methionine oxidation and *N*-acetylation of protein N-termini were set as variable modifications. In the case of FASP-digested samples, carbamidomethylation of cysteines was set as a static modification. Peptide spectrum matches (PSMs) were filtered using the Percolator node to satisfy a false discovery rate (FDR) of 0.01 (based on *q*-values). Subsequently, identifications were filtered to achieve a peptide and protein level FDR of 0.01. $MS^1$ features were determined using the Minora node with default settings. LC-MS/MS runs were chromatographically aligned with a maximum retention time drift of 10 min. Protein ratios were calculated as the median of all possible pairwise ratios of connected unique and razor peptides.

**Flow cytometry gating strategy and FRET analysis**

Forward versus side scatter (FSC vs. SSC) plots were used to define intact cells, and doublets were excluded by plotting the height versus area of FSC for subsequent FRET analysis. Fluorescence emission was detected by excitation at 405 nm using bandpass (BP) filters 450/40 nm (donor emission) and 525/50 nm (FRET emission) and excitation at 488 nm using the BP filter 530/30 nm (acceptor emission). The gates were uniformly applied to all experiments and different negative controls (nontransfected cells, all constructs as single transfections, and all constructs in combination with unfused Cer or unfused EYFP, respectively) were included to ensure gate stringency (Supplementary Figure 8). Data were analyzed using Flowing Software v2.5.1 and relative FRET efficiency was calculated from gate 4 (plot FRET vs. Donor, Supplementary Figure 8) for three independent samples for each combination.

## REFERENCES


1. Post J, van Deenen N, Fricke J, Kowalski N, Wurbs D, Schaller H, Eisenreich W, Huber C, Twyman RM, Prüfer D, Gronover CS. Laticifer-specific cis-prenyltransferase silencing affects the rubber, triterpene, and inulin content of Taraxacum brevicorniculatum. Plant Physiol. 2012; 158:1406–17. https://doi.org/10.1104/pp.111.187880 PMID:22238421

2. Bevan M. Binary Agrobacterium vectors for plant transformation. Nucleic Acids Res. 1984; 12:8711–21. https://doi.org/10.1093/nar/12.22.8711 PMID:6095209

3. Töpfer R, Matzeit V, Gronenborn B, Schell J, Steinbiss HH. A set of plant expression vectors for transcriptional and translational fusions. Nucleic Acids Res. 1987; 15:5890. https://doi.org/10.1093/nar/15.14.5890 PMID:3615207

4. Bischof J, Maeda RK, Hediger M, Karch F, Basler K. An optimized transgenesis system for Drosophila using germ-line-specific phiC31 integrases. Proc Natl Acad Sci U S A. 2007; 104:3312–7. http://www.pnas.org/cgi/doi/10.1073/pnas.0611511104 https://doi.org/10.1073/pnas.0611511104 PMID:17360644

5. Horsch RB, Klee HJ, Stachel S, Winans SC, Nester EW, Rogers SG, Fraley RT. Analysis of Agrobacterium tumefaciens virulence mutants in leaf discs. Proc Natl Acad Sci U S A. 1986; 83:2571–5. https://doi.org/10.1073/pnas.83.8.2571 PMID:3458219

6. Hoekema A, Hirsch PR, Hooykaas PJJ, Schilperoort RA. A binary plant vector strategy based on separation of *vir*- and T-region of the *Agrobacterium tumefaciens* Ti-plasmid. Nature. 1983; 303:179–80. https://doi.org/10.1038/303179a0

7. Clough SJ, Bent AF. Floral dip: a simplified method for Agrobacterium-mediated transformation of Arabidopsis thaliana. Plant J. 1998; 16:735–43. https://doi.org/10.1046/j.1365-313x.1998.00343.x PMID:10069079

8. Walter M, Chaban C, Schütze K, Batistic O, Weckermann K, Näke C, Blazevic D, Grefen C, Schumacher K, Oecking C, Harter K, Kudla J. Visualization of protein interactions in living plant cells using bimolecular fluorescence complementation. Plant J. 2004; 40:428–38. https://doi.org/10.1111/j.1365-313X.2004.02219.x PMID:15469500

9. Wiśniewski JR, Zougman A, Nagaraj N, Mann M. Universal sample preparation method for proteome analysis. Nat Methods. 2009; 6:359–62. https://doi.org/10.1038/nmeth.1322 PMID:19377485

10. Rappsilber J, Mann M, Ishihama Y. Protocol for micro-purification, enrichment, pre-fractionation and storage of peptides for proteomics using StageTips. Nat Protoc. 2007; 2:1896–906. https://doi.org/10.1038/nprot.2007.261 PMID:17703201

11. Shevchenko A, Tomas H, Havlis J, Olsen JV, Mann M. In-gel digestion for mass spectrometric characterization of proteins and proteomes. Nat Protoc. 2006; 1:2856–60. https://doi.org/10.1038/nprot.2006.468 PMID:17406544

12. Waterhouse A, Bertoni M, Bienert S, Studer G, Tauriello G, Gumienny R, Heer FT, de Beer TAP, Rempfer C, Bordoli L, Lepore R, Schwede T. SWISS-MODEL: homology modelling of protein structures and complexes. Nucleic Acids Res. 2018; 46:W296–303.
https://doi.org/10.1093/nar/gky427
PMID:29788355

## Supplementary Figures

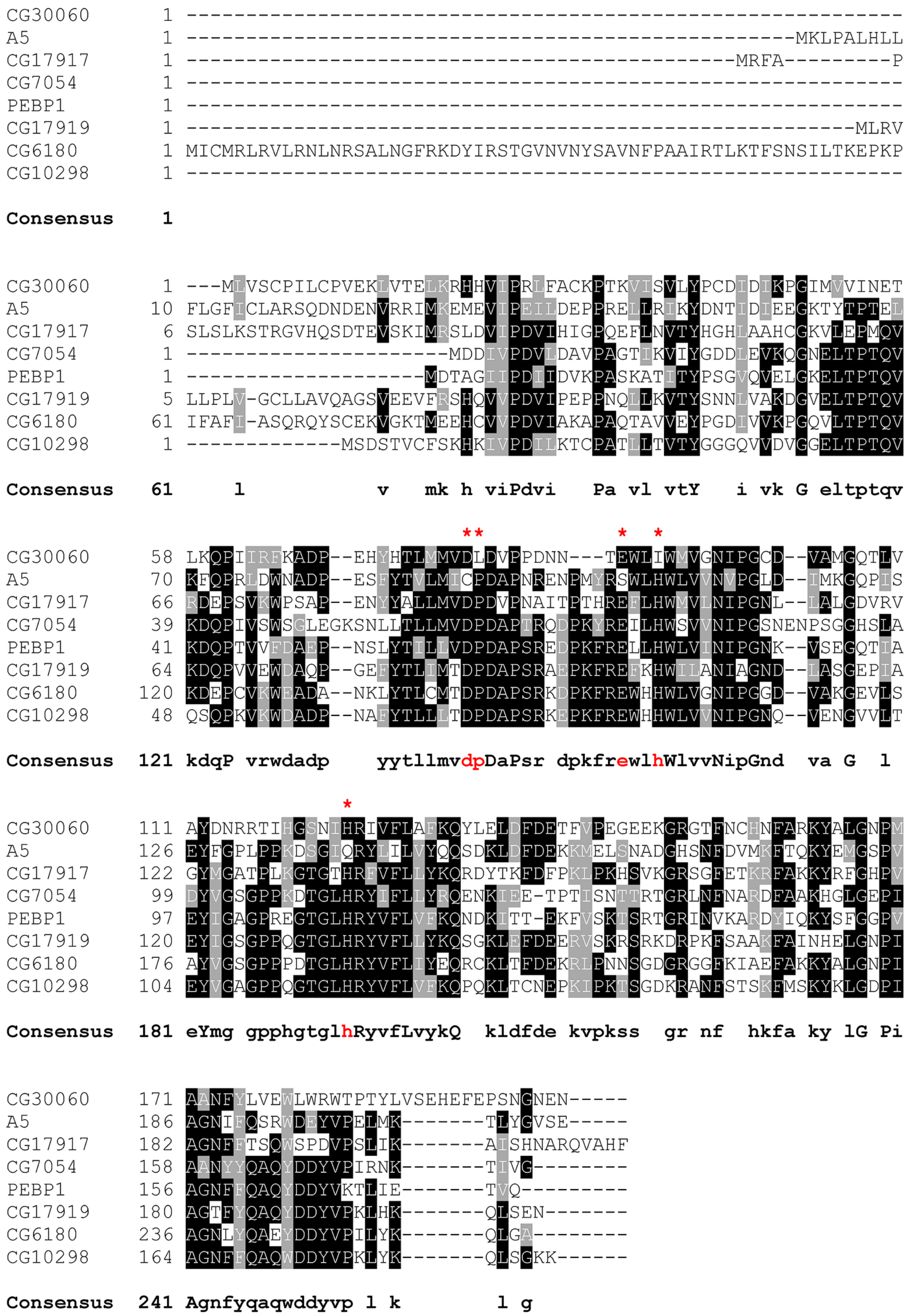


**Supplementary Figure 1. Protein sequence alignment of the eight Drosophila PEBP-like proteins.** Alignment of CG30060 (NP_725293.1), A5 (NP_476998.1), CG17917 (NP_649642.1), CG7054 (NP_651050.1), PEBP1 (NP_651051.1), CG17919 (NP_649644.1), CG6180 (NP_609588.1) and CG10298 (NP_649643.1) using Clustal Omega (https://www.ebi.ac.uk/Tools/msa/clustalo/). Box shading represents identical amino acids (black) and similar amino acids (gray), with at least 50% of the sequences carrying the corresponding amino acids (BOXSHADE v3.21). Red letters and asterisks indicate variations in the conserved motifs of the phosphatidylethanolamine-binding pocket in proteins A5 and CG30060.

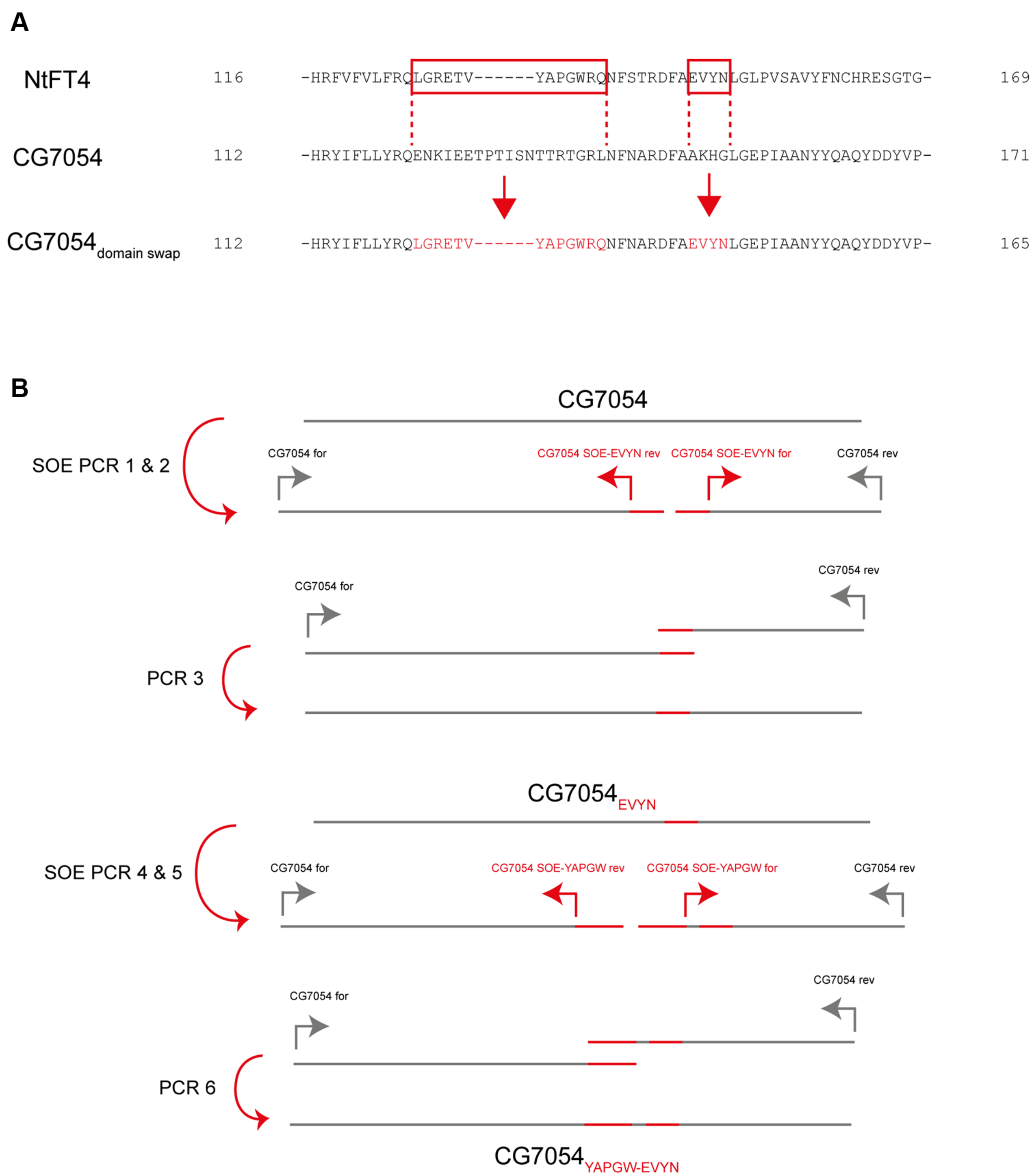


**Supplementary Figure 2. Splice overlap extension (SOE)-PCR scheme for the creation of the CG7054-DS sequence encoding a chimeric CG7054 protein with NtFT4 domains.** (**A**) Alignment of the CG7054 and NtFT4 segments that were exchanged in CG7054-DS. Motifs that are necessary for floral activators (NtFT4, red boxes) were used to replace the corresponding region of CG7054, allowing the expression in tobacco of an animal PEBP which contains conserved motifs for floral transition (red letters). (**B**) Steps and primers used to introduce segments of tobacco NtFT4 into Drosophila CG7054 by SOE-PCR. Red parts represent overhangs added during SOE-PCR steps 1 and 2, and steps 4 and 5, which subsequently align in the fragment templates for steps 3 and 6 to generate the full-length CG7054-DS ($CG7054_{YAPGW\text{-}EVYN}$).

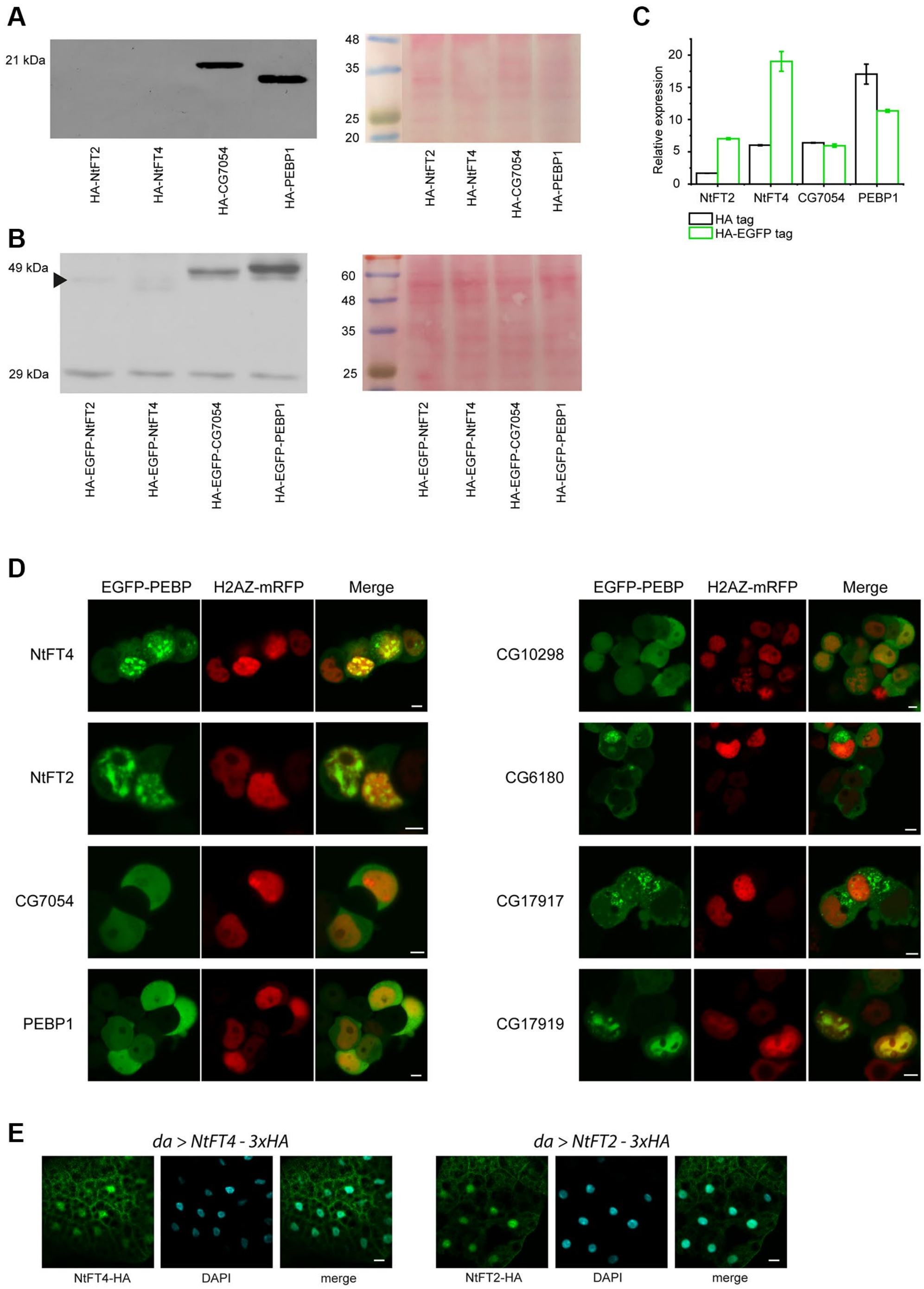


**Supplementary Figure 3. Transient expression of tagged PEBPs in S2 and HEK-293T cells.** (**A**) Western blot of transiently expressed HA-NtFT2, HA-NtFT4, HA-CG7054 and HA-PEBP1 in S2 cells. HA-tagged proteins were detected using a rabbit anti-HA antibody and comparable protein loading and transfer were confirmed by staining with Ponceau S. (**B**) Western blot of transiently expressed HA-EGFP-NtFT2, HA-EGFP-NtFT4, HA-EGFP-CG7054 and HA-EGFP-PEBP1 in S2 cells. HA-EGFP-tagged proteins were detected using a rabbit anti-HA antibody and comparable protein loading and transfer were tested by staining with Ponceau S. Cleaved HA-EGFP was also detected at ~29 kDa. The weak bands representing HA-EGFP-NtFT2 and the adjacent HA-EGFP-NtFT4 are indicated by the arrowhead. (**C**) Expression levels were simultaneously determined by quantitative RT-PCR. Relative expression levels were calculated for HA (black) and HA-EGFP (green) fusion constructs in relation to *Gapdh2*. Data are means ± SEM ($n$ = 3). (**D**) Confocal images showing the subcellular localization of EGFP-PEBP fusion proteins expressed in HEK-293T cells. The cells were transiently transfected with EGFP-PEBP (NtFT4, NtFT2, CG7054, PEBP1, CG10298, CG6180, CG17917, CG17919) and H2AZ-mRFP (red) constructs and analyzed 1 d post-transfection. Scale bar = 5 µm. (**E**) UAS-NtFT4-3xHA and UAS-NtFT2-3xHA flies were mated with the da-Gal4 driver strain to detect the expression of tobacco PEBPs NtFT4 and NtFT2 in Drosophila. Proteins were detected in fat body cells by immunostaining using an anti-HA mouse monoclonal antibody (green). Nuclei were counterstained with DAPI (blue). Scale bar = 20 µm.

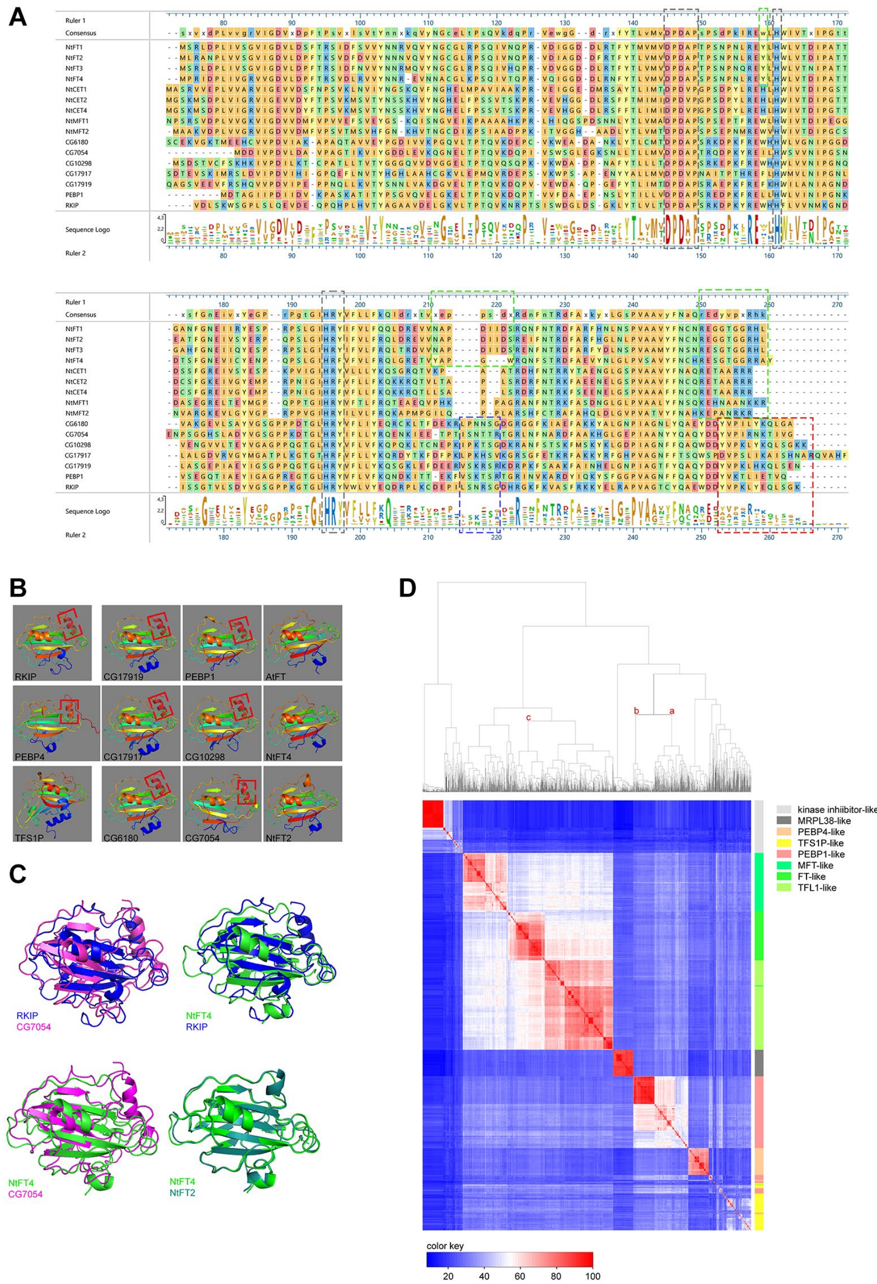


**Supplementary Figure 4. Sequence and 3D structure of tobacco and Drosophila PEBPs.** (**A**) Peptide sequences of NtFT1, NtFT2, NtFT3, NtFT4, NtCET1, NtCET2, NtCET4, NtMFT1, NtMFT2, CG6180, CG7054, CG10298, CG17917, CG17919, PEBP1 and human RKIP were aligned using MegAlign Pro (DNAStar) and Clustal Omega. Conserved amino acids are indicated by letter size in the sequence logo. Characteristic motifs are enclosed in dashed boxes (gray = conserved PEBP motifs, green = plant PEBP motifs of floral regulators, blue = major differences between animal and plant PEBPs in the loop region, red = C-terminal α helix of animal PEBPs). The alignment of all eight PEBP-like proteins from Drosophila, including A5 and CG30060, is shown in Supplementary Figure 11. (**B**) The 3D protein structures of human RKIP and PEBP4, yeast TFS1P, Drosophila CG17919, CG17917, CG6180, PEBP1, CG10298, CG7054, Arabidopsis FT and tobacco NtFT4 and NtFT2. The crystal structures of RKIP, PEBP4, TFS1P, CG7054 and FT are known and the other PEBPs were predicted using Swiss-MODEL [12]. The red boxes indicate the C-terminal α-helix of animal PEBPs. Coloring indicates the N-terminus (blue) to the C-terminus (red). (**C**) Aligned 3D structures of RKIP (blue) with CG7054 (magenta) or NtFT4 (green) and of NtFT4 (green) with CG7054 (magenta) and NtFT2 (turquoise). (**D**) Heat map identity matrix of 1596 PEBPs from species ranging from prokaryotes to mammals and plants. PEBP sequences were aligned using Clustal Omega and the output identity matrix was plotted as a heat map using R Studio v1.3.1093. Color coding represents identities ranging from low (blue) to high (red) in percent identity. PEBPs were assigned to prokaryotic *kinase inhibitor-like* (light gray), to *TFS1P-like* (yellow), *MRPL38-like* (gray), *PEBP1-like* (light red), *PEBP4-like* (orange), plant *MFT-like* (blue-green), *TFL1-like* (yellow-green) and *FT-like* (green) indicated at the top. In the dendrogram *a* indicates the PEBP1 cluster, in which all Drosophila PEBPs can be found, *b* indicates the highly-conserved mammalian PEBP1-like proteins and *c* indicates the plant FT-like subgroup in which tobacco NtFT4 and NtFT2 are found.

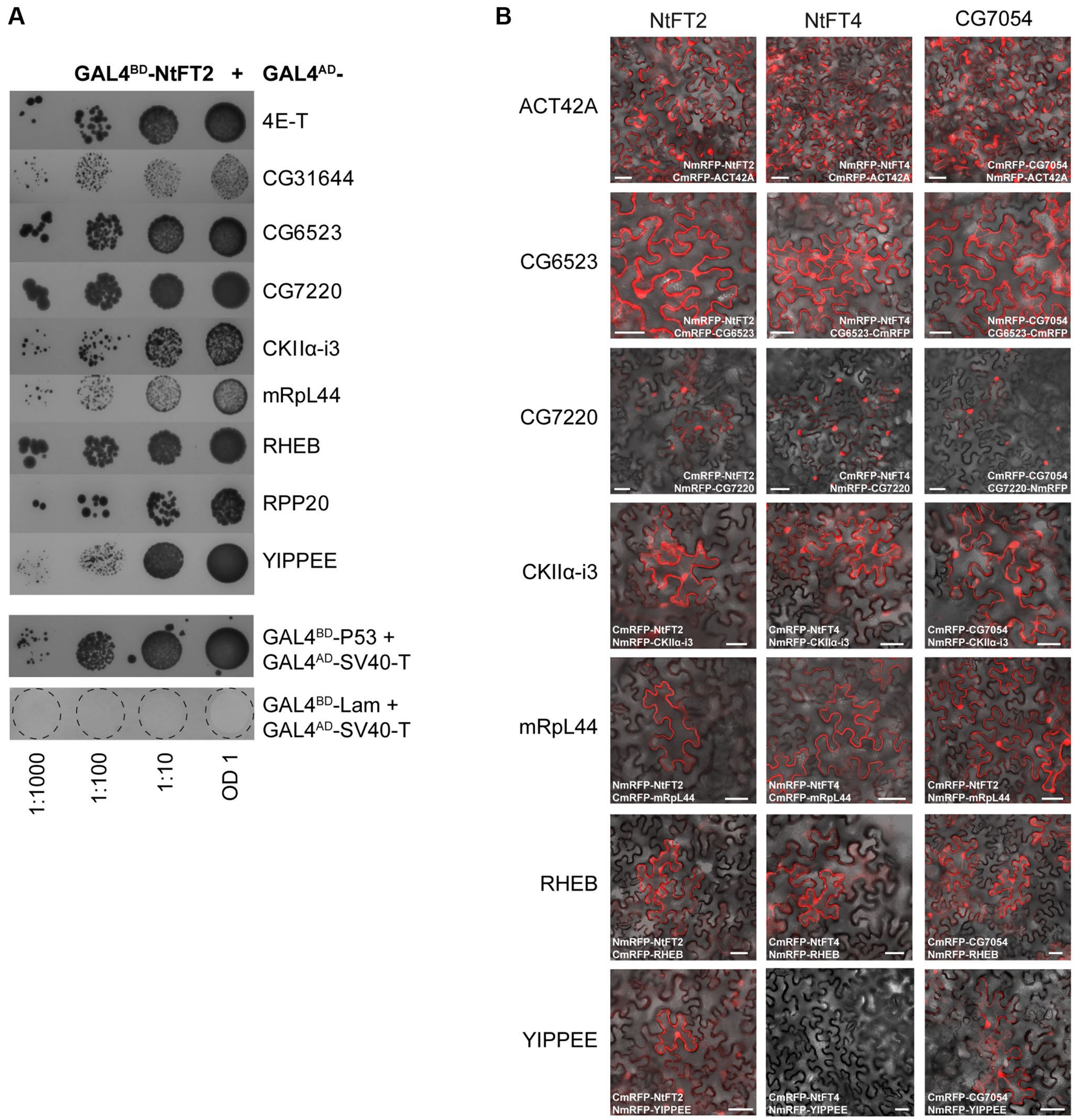


**Supplementary Figure 5. Interaction partners of NtFT2, NtFT4 and CG7054 identified by yeast-two hybrid screening of a normalized Drosophila cDNA library.** (**A**) Coding sequences of putative interaction partners fused to the Gal4 activation domain ($Gal4^{AD}$) and a bait construct comprising the Gal4 binding domain ($Gal4^{BD}$) fused to NtFT2 were simultaneously introduced into *S. cerevisiae* strain Y2HGold for drop tests on selective plates. The interaction of murine p53 with the large T-antigen (SV40-T) served as a positive control, whereas the combination of lamin with SV40-T served as a negative control. The different dilutions of yeast suspensions (undiluted, 1 :10, 1 :100 and 1 :1000) are indicated. The interaction of NtFT2 with Act42 was not tested due to growth defects of the prey strain expressing Act42A. The interaction with NtFT4 was not tested in yeast due to auto-activation of the bait strain expressing Gal4-BD-NtFT4. (**B**) Bimolecular fluorescence complementation (BiFC) in *N. benthamiana* leaf epidermal cells to confirm the interaction with NtFT2 in a different background and analyze the interaction with NtFT4 and CG7054. Representative merged bright-field and fluorescence images are shown and the corresponding split-mRFP constructs used for co-transformation are indicated. BiFC provided unclear results for the interactions with 4E-T and CG31644. Scale bars = 50 µm.

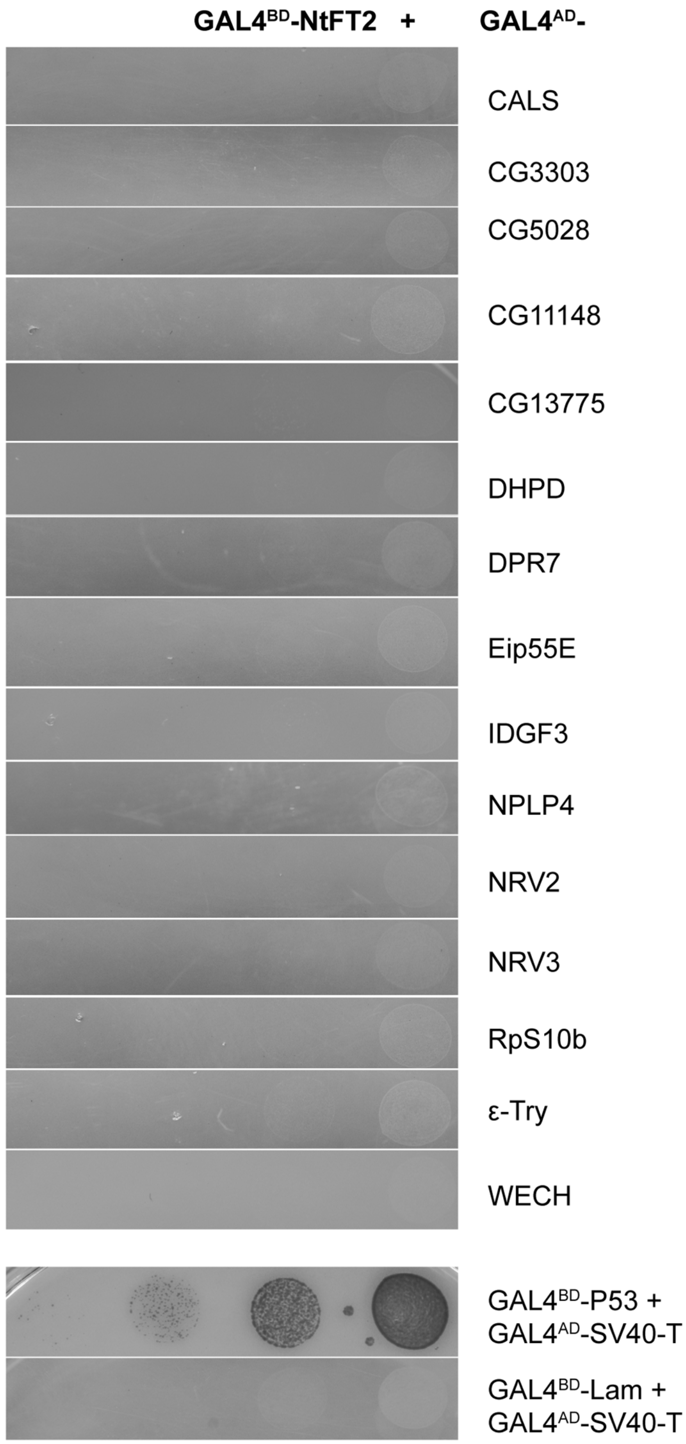


**Supplementary Figure 6. Putative interaction partners of NtFT2 identified in the yeast two-hybrid screen which were not confirmed in drop tests with the full-length coding sequences.** Coding sequences of putative interaction partners in fusion with the Gal4 activation domain ($Gal4^{AD}$) were introduced into *S. cerevisiae* Y2HGold cells with the bait construct comprising the Gal4 binding domain ($Gal4^{BD}$) fused to NtFT2 for drop tests on selective plates. The interaction of murine p53 with the large T-antigen (SV40-T) served as a positive control, and the combination of lamin with SV40-T served as a negative control. The different dilutions of yeast suspensions (undiluted, 1 :10, 1 :100 and 1 :1000) are indicated.

A

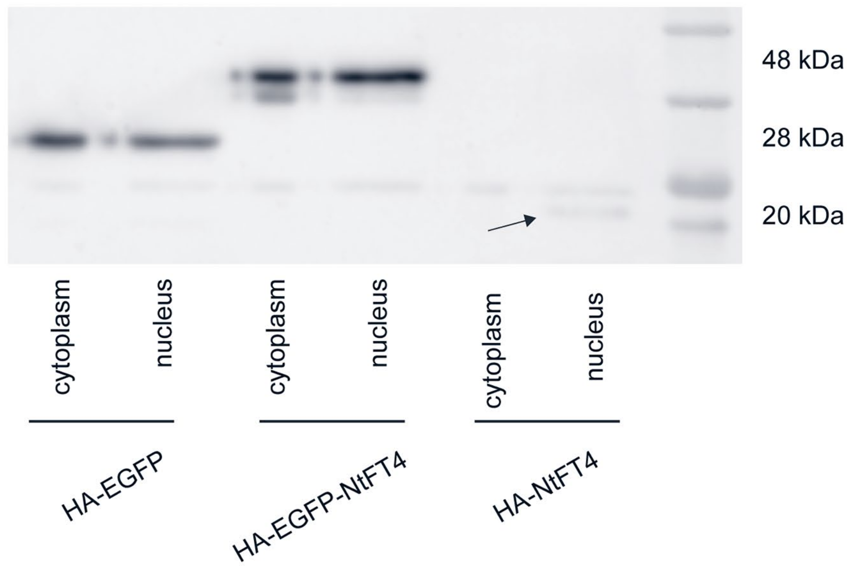


B

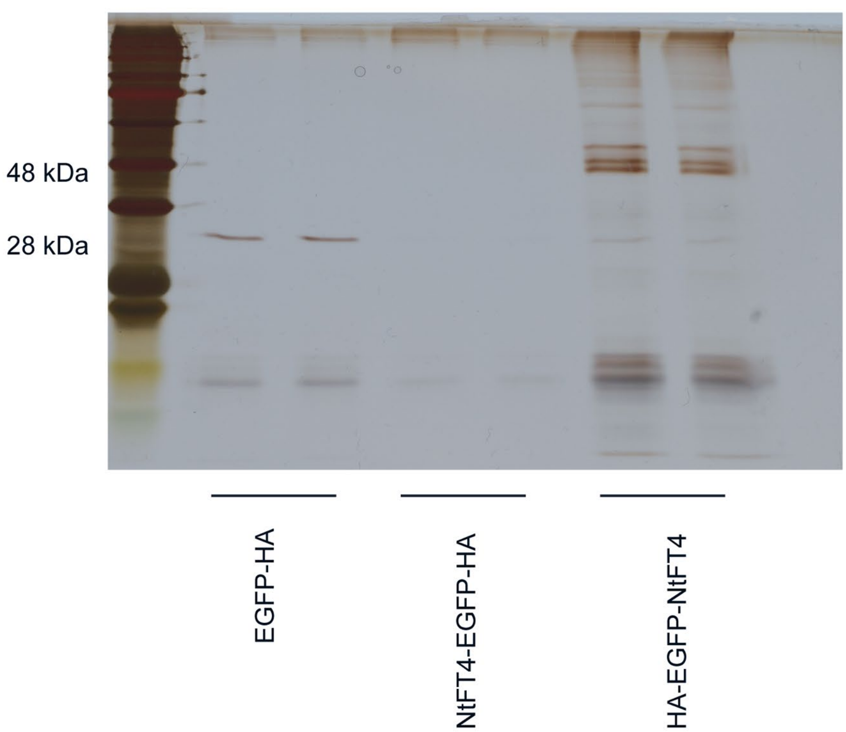


**Supplementary Figure 7. Detection of tagged and codon-optimized NtFT4 expressed in S2 cells and immunoprecipitation to identify interaction partners in flies.** (**A**) Different extraction protocols were tested to extract sufficient amounts of NtFT4 for immunoprecipitation. Western blot of transiently expressed HA-EGFP, HA-EGFP-NtFT4 and HA-NtFT4 in the cytoplasmic and nuclear protein fractions. The arrow indicates a weak band corresponding to HA-NtFT4 in the nuclear fraction. (**B**) Silver staining of eluates of different HA-tagged bait proteins after immunoprecipitation. Transiently expressed HA-EGFP-NtFT4, NtFT4-EGFP-HA and HA-EGFP were extracted in separate cytoplasmic and nuclear fractions as above and both fractions were combined for immunoprecipitation. Because eluates using NtFT4-EGFP-HA showed only traces of protein bands, these samples were not processed any further. Regions showing distinct bands in the eluates of HA-EGFP-NtFT4 were excised and both these gel pieces and the complete eluates were analyzed by LC-MS/MS compared to the corresponding samples of the HA-EGFP eluates.

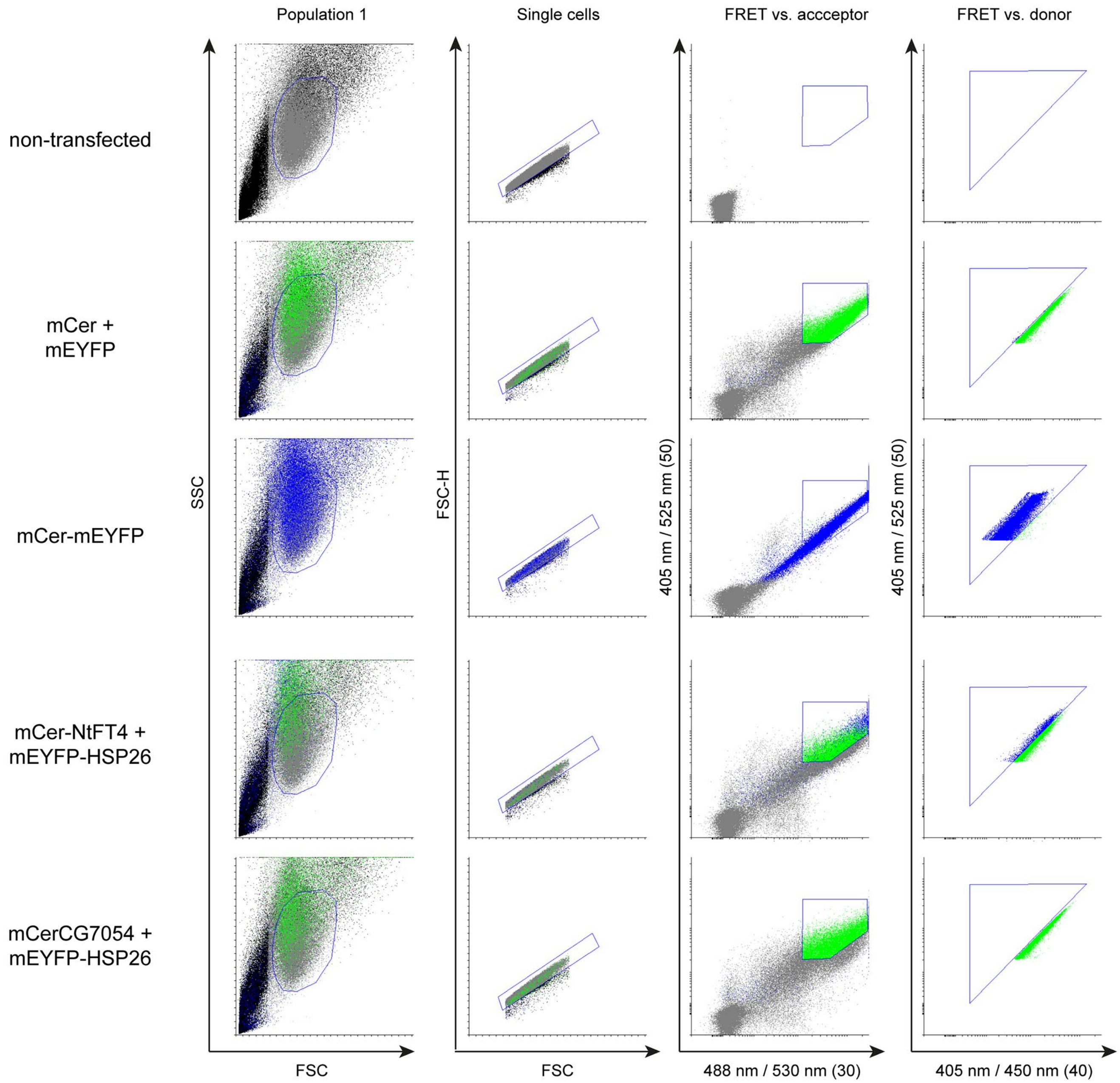


**Supplementary Figure 8. Gating strategy for FRET analysis by flow cytometry.** All samples were gated using the same settings and representative samples are shown. Single cells were gated using FSC and SSC to define intact cell population 1, and the area (FSC-A) and height (FSC-H) of FSC to exclude doublets. Single cells were then plotted for events identified by excitation at 405 nm and detection at 525 (50) nm against excitation at 488 nm and detection at 530 (30) nm (FRET vs. acceptor). The distinct population with emissions at both excitation wavelengths was then plotted for events identified by excitation at 405 nm and detection at 525 (50) nm against excitation at 405 nm and detection at 450 (40) nm (FRET vs. donor, quantification gate for FRET efficiency). The gate to quantify only FRET-positive cells was set using all negative controls included in the experiments expressing both fluorophores (Cer + EYFP, Cer-PEBP + EYFP, Cer + EYFP-POI), in which < 0.5% events of the parental gate could be detected. A protein fusion of mCer-mEYFP served as positive control with maximum FRET activity. Abbreviation: POI: protein of interest.

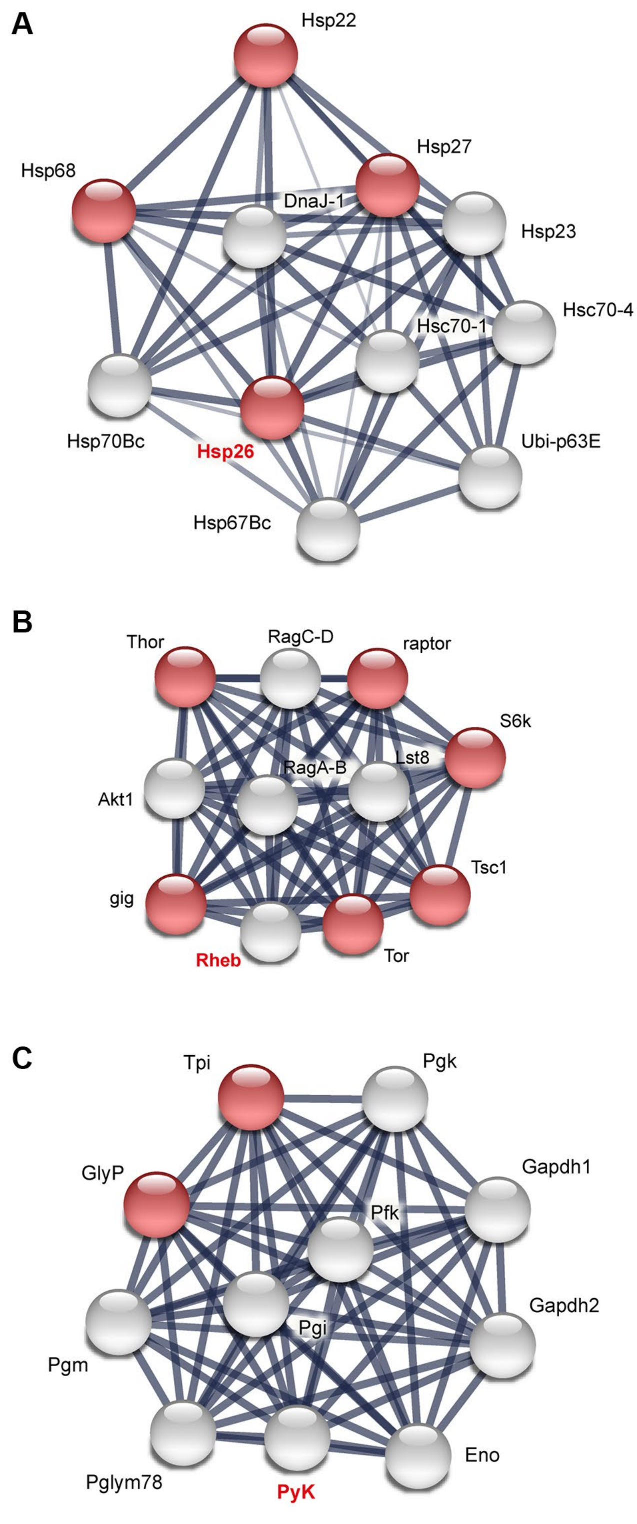


**Supplementary Figure 9. Interaction networks of HSP26, RHEB and PyK, which are associated with lifespan determination.** (**A**) Predicted interaction network of HSP26 in Drosophila. HSP26 is associated with several other heat shock proteins and HSP26 itself was shown to influence longevity in Drosophila. (**B**) Predicted interaction network of RHEB in Drosophila. RHEB is associated with several proteins in the IIS/TOR signaling pathway, which were shown to determine lifespan in different model organisms. RHEB itself is not yet directly linked to the determination of lifespan. (**C**) Predicted interaction network of PyK in Drosophila. PyK was shown to influence lifespan in nematodes [34] but is also likely to influence lifespan through triose phosphate isomerase (Tpi) and glycogen phosphorylase (GlyP). Red nodes indicate proteins related to the determination of lifespan by direct experimental evidence or if orthologs in other species were found to alter lifespan (https://string-db.org). Brightness and thickness of lines correspond to the confidence of an interaction.

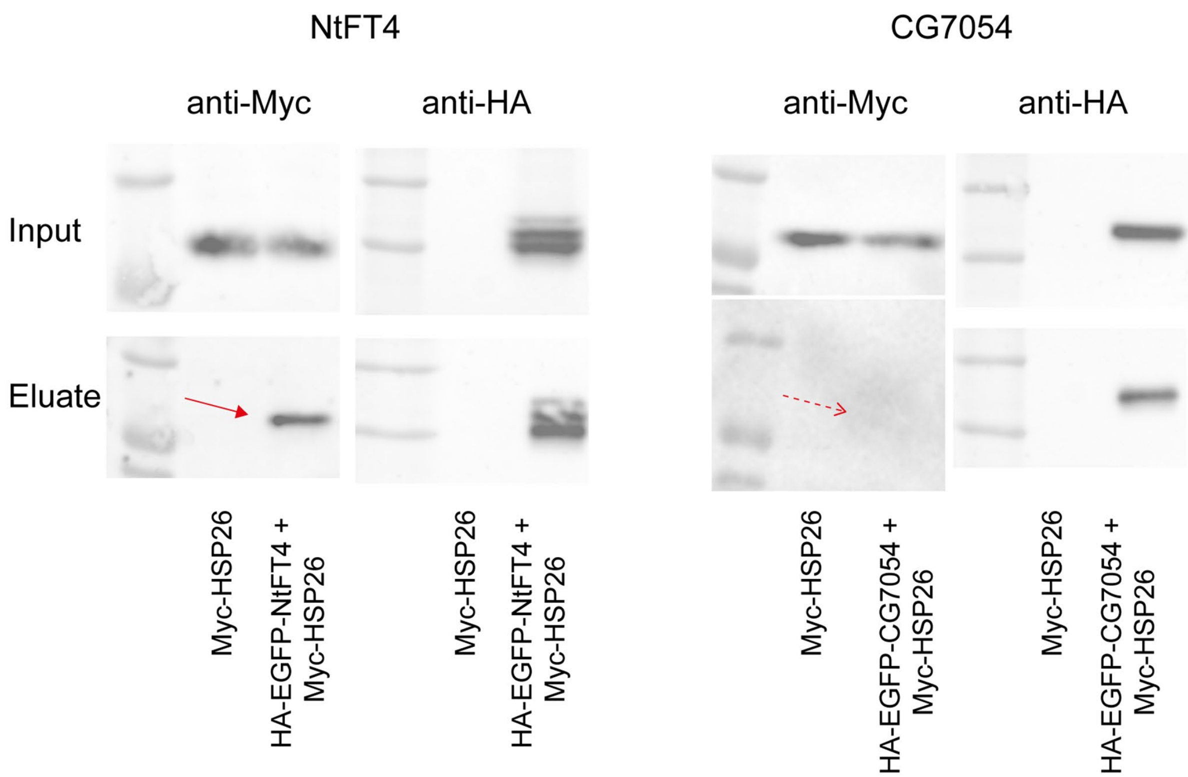


**Supplementary Figure 10. Co-immunoprecipitation shows that HSP26 interacts with NtFT4 but not CG7054.** A Myc-tagged HSP26 was transiently expressed with HA-EGFP-NtFT4 or HA-EGFP-CG7054 in S2 cells. Protein extracts from single transfections (Myc-HSP26) and double transfections (Myc-HSP26 with HA-EGFP-NtFT4 or HA-EGFP-CG7054) were precipitated using magnetic anti-HA beads and the eluates and the input extracts were analyzed by Western blot using mouse anti-Myc and rabbit anti-HA antibodies. Myc-HSP26 was only detected in eluates using HA-EGFP-NtFT4 as the bait (solid arrow), whereas no band was detected in eluates using HA-EGFP-CG7054 as the bait (dashed arrow).

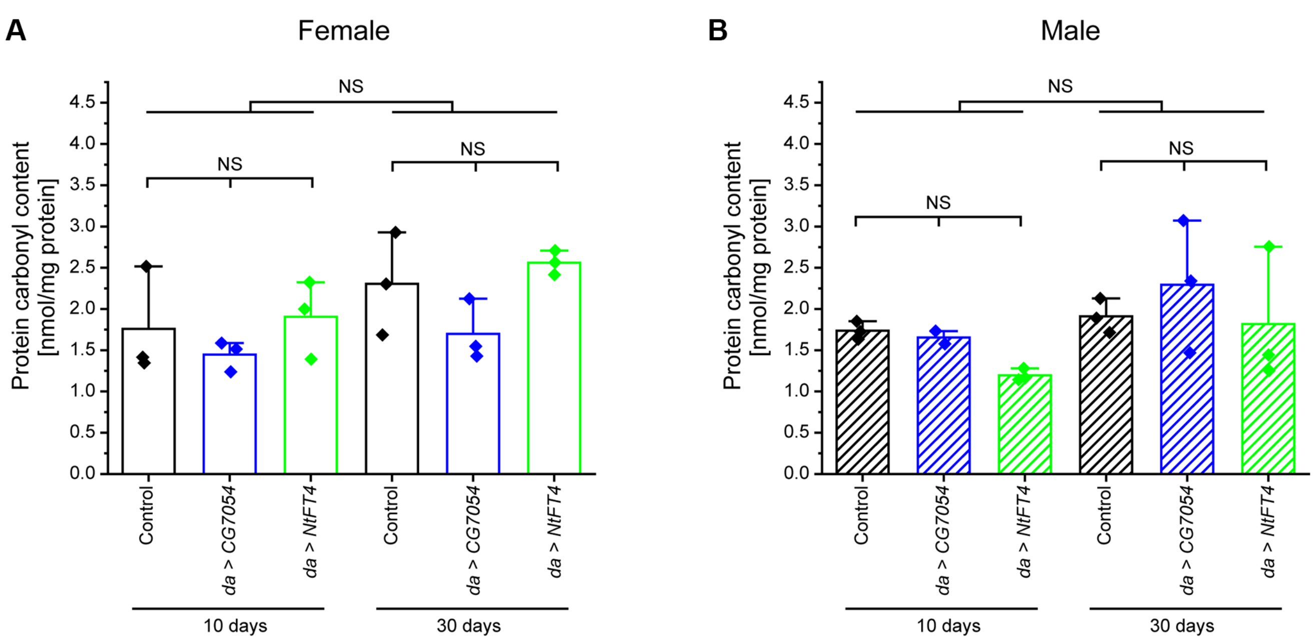


**Supplementary Figure 11. Protein carbonylation in *da > CG7054* and *da > NtFT4* flies.** Carbonyl content in protein extracts of female (**A**) and male (**B**) flies (10 or 30 days old) expressing CG7054 or NtFT4 after mating UAS-NtFT4 or UAS-CG7054 with the *da-Gal4* driver strain compared with *da-Gal4* x Oregon-R (control). Data are means ± SEM (*n* = 3, except for *da > CG7054* ♂ 10 days). Significance was tested by one-way ANOVA and Tukey's post hoc test. Abbreviations: *NS*: not significant.

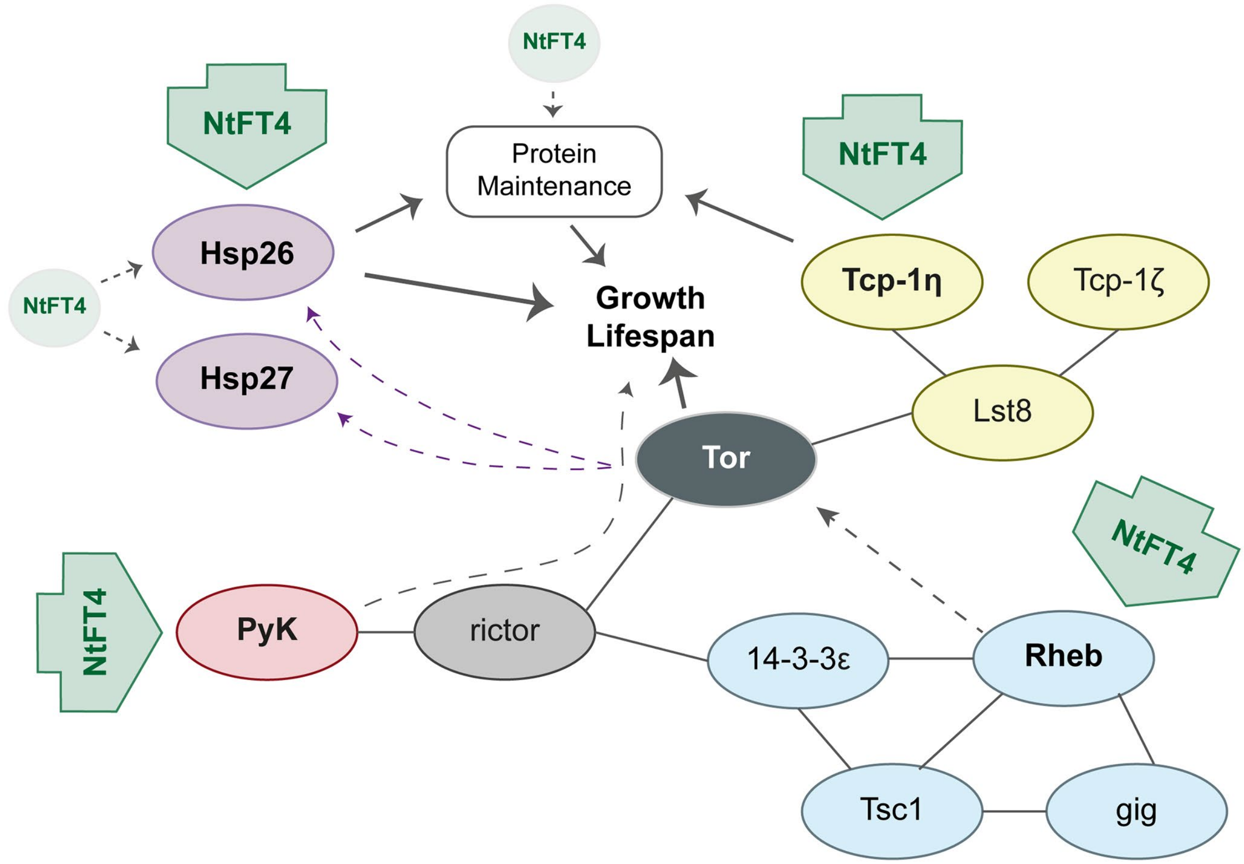


**Supplementary Figure 12. Overview of NtFT4 interactions that intersect with IIS/TOR signaling in Drosophila.** Physical interactions between NtFT4 and RHEB, CCT7 (Tcp-1η), PyK and HSP26 are indicated by green arrows. HSP26 and PyK have immediate (solid arrow) or indirect (dashed arrow) functions in the determination of lifespan. RHEB and CCT7 act through their association with TOR. Physical or genetic interactions with components of the IIS/TOR network are indicated by solid lines. NtFT4 also influences the regulation of *Hsp26* and *Hsp27* gene expression (NtFT4 in green circles) and of proteases which could contribute to protein maintenance and homeostasis. Protein maintenance is also influenced by CCT7 and the heat shock proteins.

## Supplementary Tables

**Supplementary Table 1. Survival of male flies with dysregulated PEBP expression [*da-Gal4/UAS-CG7054*, *da-Gal4/UAS-NtFT2* or *da-Gal4/UAS-NtFT4*)] or [*da-Gal4/UASt-CG7054*$^{dsRNA}$] compared with the control +/*da-Gal4*.**

| | median lifespan [d] | 25 % estimate [d] | mean lifespan [d] | Equality vs. Control ($\chi^2$) | Equality vs. CG7054 ($\chi^2$) | Equality vs. NtFT2 ($\chi^2$) |
|---|---|---|---|---|---|---|
| **Control** | 42 | 40 | 39.83 (± 0.53) | - | - | - |
| **CG7054** | 47 | 40 | 43.28 (± 0.66) | 55.51 ($p = 9.31 \times 10^{-14}$) | - | - |
| **CG7054$^{dsRNA}$** | 25 | 7 | 19.95 (± 0.83) | 330.66 ($p = 0$) | 351.66 ($p = 0$) | - |
| **NtFT2** | 40 | 30 | 36.93 (± 0.93) | 1.05 ($p = 0.31$) | 11.99 ($p = 5.36 \times 10^{-4}$) | - |
| **NTFT4** | 47 | 37 | 42.7 (± 0.67) | 41.22 ($p = 1.36 \times 10^{-10}$) | 0.008 ($p = 0.93$) | 10.98 ($p = 9.19 \times 10^{-4}$) |

Median lifespans, 25% quartile estimates and mean lifespans were calculated based on Kaplan-Meier survival curves, and $\chi^2$ and *p*-values were calculated using the Mantel-Cox method.

**Supplementary Table 2. Overview of NtFT4 putative interaction partners identified by immunoprecipitation with HA-EGFP-NtFT4.**

| Name | Abundance ratio (HA-EGFP-NtFT4 / HA-EGFP) | Confirmed (method) |
|---|---|---|
| Cbs | 100.0 | no |
| CCT2 | 100.0 | yes (Co-IP) |
| CCT3 | 100.0 | no |
| CCT5 | 100.0 | no |
| CCT6 | 100.0 | no |
| CCT7 | 100.0 | yes (Co-IP, FRET) |
| Inos | 100.0 | no |
| p47 | 100.0 | yes (Co-IP) |
| Pen | 100.0 | yes (Co-IP, FRET) |
| Stip1 | 100.0 | no |
| tudor-SN | 100.0 | yes (Co-IP, FRET) |
| Hsp26 | 71.4 | yes (Co-IP, FRET) |
| Rack1 | 28.1 | no |
| Df31 | 21.3 | yes (BiFC) |
| eEF1beta | 16.1 | no |
| PyK | 14.7 | yes (Co-IP, FRET) |
| 14-3-3zeta | 13.0 | no |
| CG4364 | 7.4 | yes (Co-IP, FRET) |
| CG32549* | 100.0 | nd |
| Akap200* | 100.0 | nd |

| | | |
|---|---|---|
| SerRS* | 100.0 | nd |
| CG12128* | 100.0 | nd |
| AspRS* | 100.0 | nd |

HA-EGFP-NtFT4 and HA-EGFP were transiently expressed in S2 cells and nuclear and cytoplasmic proteins were precipitated using magnetic anti-HA beads. Eluted proteins were analyzed by LC-MS/MS and the protein abundance ratio was calculated by comparing HA-EGFP-NtFT4 and HA-EGFP eluates. An abundance ratio of 100 was specified if no peptides corresponding to this protein were detected in the HA-EGFP eluate. Protein interactions were also analyzed by co-immunoprecipitation in co-transfected S2 or HEK-293T cells (Co-IP) or by fluorescence resonance energy transfer (FRET) analysis of transfected HEK-293T cells. *Putative interaction partners that were not analyzed (nd).

**Supplementary Table 3. Correlation analysis of expression profiles of female *da-Gal4* and *da > NtFT4* flies.**

| Sample | | *da-Gal4* | | | *da > NtFT4* | | |
|---|---|---|---|---|---|---|---|
| | | **Pool 1** | **Pool 2** | **Pool 3** | **Pool 1** | **Pool 2** | **Pool 3** |
| | **Pool 1** | ***1.000*** | 0.982 | 0.983 | *0.974* | *0.973* | 0.978 |
| ***da-Gal4*** | **Pool 2** | 0.982 | ***1.000*** | 0.995 | 0.983 | 0.996 | 0.997 |
| | **Pool 3** | 0.983 | 0.995 | ***1.000*** | 0.981 | 0.992 | 0.994 |
| | **Pool 1** | *0.974* | 0.983 | 0.981 | ***1.000*** | 0.982 | 0.987 |
| ***da > NtFT4*** | **Pool 2** | *0.973* | 0.996 | 0.992 | 0.982 | ***1.000*** | 0.998 |
| | **Pool 3** | 0.978 | 0.997 | 0.994 | 0.987 | 0.998 | ***1.000*** |

Similarity of the expression profiles of samples was determined by calculating Pearson's correlation coefficient *r* using GeneSpring GX v13.1. The correlation coefficients of all possible comparisons range from 0.973 to 0.998. The high correlation between all samples suggests that their global gene expression profiles may be very similar. The color range shows correlation coefficients from the lowest value of r ~ 0.97 (Italic) through to r = 1.00 (Bold Italic).

**Supplementary Table 4. Number of deregulated genes in female flies expressing NtFT4 (*da-Gal4 > UAS-NtFT4*) vs. control flies (*da-Gal4*).**

| | **FC > 1.5 $p < 0.05$** | **FC > 1.5** |
|---|---|---|
| **Upregulated** | 49 | 135 |
| **Downregulated** | 100 | 208 |
| **Total** | 149 | 343 |

Female flies aged 1, 5 and 10 days were pooled for whole-transcriptome analysis and flies expressing *NtFT4* were compared to control flies (*da-Gal4* x Oregon-R) using GeneChip Drosophila Genome 2.0 arrays (Affymetrix). Differential gene expression was calculated by pairwise comparison of averaged normalized signal values ($n$ = 3). All genes with a fold-change (FC) > 1.5 and a $p$-value < 0.05 ($t$-test) are listed in the second column, and all genes with a FC > 1.5 including non-significant events are listed in the third column. A total of 18,952 probes was analyzed on the GeneChip.

Please browse Full Text version to see the data of Supplementary Tables 5 to 9.

**Supplementary Table 5. Differentially expressed genes in female *da > NtFT4* flies.**

**Supplementary Table 6. Enrichment analysis of differentially expressed genes in *da > NtFT4* flies.**

**Supplementary Table 7. List of all primers used for cloning and gene expression analysis.**

**Supplementary Table 8. Accession numbers of all nucleotide and protein sequences.**

**Supplementary Table 9. The *p*-values for *t*-tests and ANOVA followed by Tukey's post hoc test.**